Shape optimization of a linearly elastic rolling structure under unilateral contact using Nitsche's method and cut finite elements.

Élie Bretin * Julien Chapelat † Pierre-Yves Outtier ‡ Yves Renard §

December 7, 2021

Abstract

The main motivation of this work is to develop a numerical strategy for the shape optimization of a rolling elastic structure under contact with respect to a uniform rolling criterion. A first objective is to highlight the influence on the treatment of the contact terms. To do so, we present a numerical comparison between a penalty-based approach and the use of Nitsche's method which is known to have good consistency properties. A second task concerns the construction of an objective functional to force the uniform rolling criterion. Here, we present and compare two different strategies that will lead to quite similar results. All the numerical experiments proposed in this paper were performed using a fictitious domain approach coupled with a level set representation of the shape and the use of a cut finite element method to approximate the elastic equation.

Key words: unilateral contact, linear elasticity, Nitsche's method, fictitious domains method, finite element method, shape optimization, level set representation.

1 Introduction

The motivation of this work is the optimization of an elastic load-bearing rolling structure under criteria of compliance and uniformity of the contact stress in a multi-loading context.

Shape optimization has become popular in recent decades for the optimal design of structures, and applications can be intricate according to the mechanical context. Difficulties might appear while differentiability of optimization criteria, which can be non-linear, can be hard to obtain in mathematical models. In this work, the elastic rolling structure is in contact with a flat ground. This generates some non-linearity and non-differentiability issues according to the contact approximation. The latter can be consistent or not, and lead to numerical imprecisions. The elastic rolling structure is optimized under mechanical criteria such as deformation and stability criteria while the structure rolls. Thereby, a multi-loading strategy simulates the rotation of the structure and leads to uniformity criteria on all the loading computations. We derive the correpsonding shape gradient and a descent strategy classically

*Univ Lyon, INSA Lyon, UJM, UCBL, ECL, CNRS UMR 5208, ICJ, F-69621, France. email: elie.bretin@insa-lyon.fr

†Univ Lyon, INSA Lyon, CNRS UMR5259, LaMCoS, F-69621, France. email: julien.chapelat@insa-lyon.fr

‡MFP MICHELIN, Campus RDI Ladoux, France. email: pierre-yves.outtier@michelin.com

§Univ Lyon, INSA Lyon, UJM, UCBL, ECL, CNRS UMR 5208, ICJ, CNRS UMR5259, LaMCoS, F-69621, France. email: yves.renard@insa-lyon.fr

based on the early ideas of J. Hadamard [24] and on later developments, such as the formulation in terms of a Lagrangian due to J. Céa [11] and the adjoint method [37] introduced by J.-L. Lions.

Our purpose is to compare two methods for the approximation of the contact condition in the shape optimization framework: the penalty approach and Nitsche's method. We also introduce two strategies to deal with the uniformity criteria while the structure is rolling. We propose numerical experiments, representing the geometry thanks to the level set method to ease its evolution as exposed by G. Allaire, F. Jouve and A.-M. Toader in [4]. We also use the finite element method to compute the mechanical problem and especially we develop the fictitious domains method [31, 10] based on cut finite elements to deal with complex geometries.

The difficulty coming from the contact boundary conditions, also called Signorini's conditions, is that they are more intricate conditions than Dirichlet and Neumann conditions. They lead to a highly non-linear problem classically set in terms of a variational inequality (at least for the frictionless case). The contact term implies a projection operator, which is, for the shape optimization, not differentiable in the usual sense. A so-called conical derivative was introduced in [39] with a derivation of the optimality conditions using a weak notion of differentiability. The shape sensitivity analysis of contact problems is analyzed in the work of J. Sokolowski and J.-P. Zolesio [51, 52]. We also refer to the work of J. Haslinger et al. [29, 30, 28, 26, 25, 27, 7] where in particular existence of an optimum is proved under assumptions of Lipschitz regularity of the boundary, from the discrete formulation to its continuous limit. A regularized approach is used in [6] and [5] and more recently [38] for different friction laws. See also the recent work [12] for the penalized approach and [13] for the augmented Lagrangian one.

We consider a rolling linearly elastic structure occupying in its reference configuration a domain $\Omega \subset \mathbb{R}^d, d = 2$ or 3 whose shape is to be optimized, an example being depicted in Figure 1. The boundary $\partial\Omega$ of the domain is split into three non-overlapping parts, Γ_N, Γ_C and Γ_D. A Neumann condition is considered on Γ_N where a force density g_N is prescribed. A contact with friction might occur with a flat and horizontal rigid obstacle on Γ_C, and a homogeneous Dirichlet condition is prescribed on Γ_D.

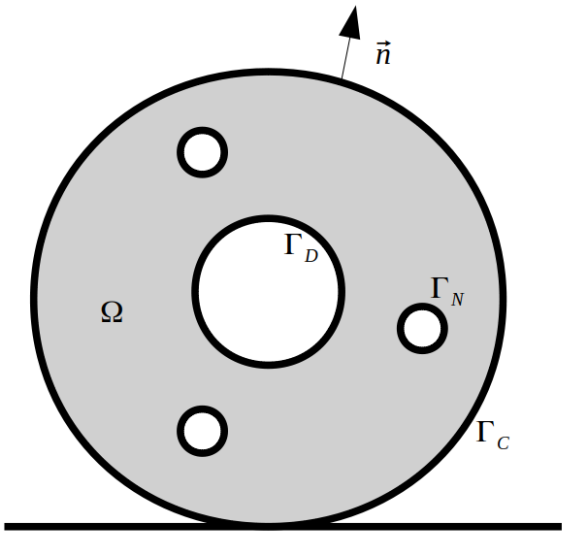

Figure 1: Schematic representation of Ω and the rigid obstacle.

The displacement $u_\Omega : \Omega \to \mathbb{R}^d$ of the body according to its reference configuration is solution to

the following linearized elasticity problem:

$$\begin{cases} \text{- div } \sigma(u_\Omega) = f & \text{in } \Omega \text{ where } \sigma(u_\Omega) = A\,\varepsilon(u_\Omega), \\ \sigma(u_\Omega)\, n \ = g_N & \text{on } \Gamma_N, \\ u_\Omega = 0 & \text{on } \Gamma_D, \end{cases} \tag{1}$$

where A is the fourth order symmetric tensor of elasticity, $\varepsilon(u)$ is the small deformations tensor, and n is the outward unit vector to Ω. The contact condition on Γ_C will be developed in the next section. Assuming the isotropy of the material, the tensor A finally reads

$$\sigma(u) = A\,\varepsilon(u) = 2\mu\varepsilon(u) + \lambda tr(\varepsilon(u))I_d, \tag{2}$$

where μ and λ are the Lamé material parameters.

For the purpose of our study, we consider that the contact and Dirichlet boundaries Γ_C and Γ_D are not some optimizable parts. However, the generalization to optimizable contact and Dirichlet boundaries is rather straightforward.

The structure is supposed to roll upon a ground (the obstacle) along its outer radius. We take this into account by considering N_l load positions, obtained as N_l rotations Ω_i of the domain Ω (see Figure 2), for i from 1 to N_l, with regularly spaced rotations of angles $i2\pi/N_l$. The displacement for the rotated domain Ω_i will be denoted u^i_Ω.

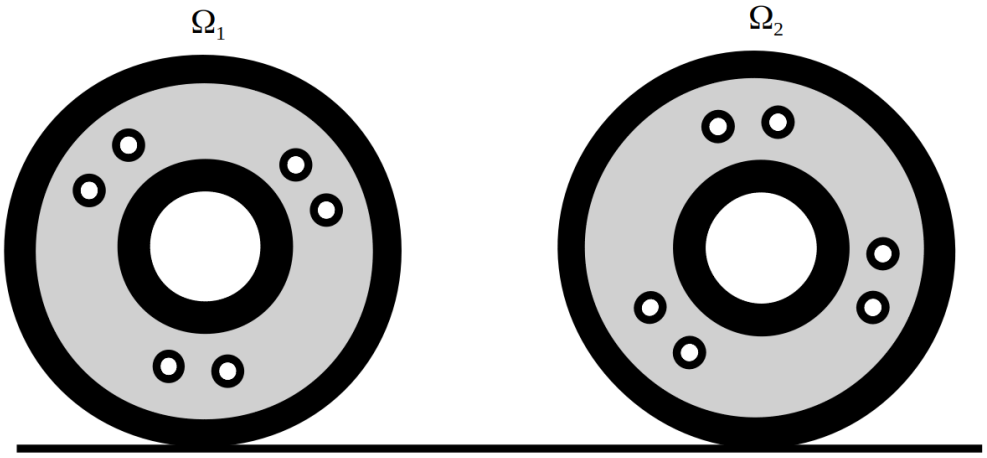

Figure 2: Rolling structure representation. Two configurations of Ω at different rotations for $i = 1, 2$.

Classically, the basic optimization criterion we consider corresponds to the strain energy, which we sum here on each load position:

$$\sum_{i=1}^{N_l} J_e(\Omega_i, u^i_\Omega) \ \text{ where } \ J_e(\Omega_i, u^i_\Omega) = \int_{\Omega_i} \frac{1}{2} A\varepsilon(u^i_\Omega) : \varepsilon(u^i_\Omega)\, \mathrm{d}x. \tag{3}$$

It aims at minimizing the energy associated to the elastic deformation corresponding to each domain Ω_i.

In order to obtain a structure that rolls as uniformly as possible, we introduce a second criterion. To this aim, we introduce the mean contact stress on the contact boundary Γ_C, where the average is obtained over the different load positions:

$$p_{mean} = \frac{1}{N_l} \sum_{i=1}^{N_l} \sigma(u^i_\Omega) n.$$

A first idea leads to minimize on each load position

$$J_p(\Omega, u_\Omega, p_{mean}) = \int_{\Gamma_C} \frac{L}{2E}(\sigma(u_\Omega)n - p_{mean})^2 \mathrm{d}s(x), \tag{4}$$

where L is a characteristic length and E is Young's modulus.

However, expression (4) is not completely satisfactory since the contact stress $\sigma(u)n$ may not be square integrable in some context and even if it is, continuity of (4) with respect to the problem data cannot be ensured. We develop in section 3.3 two more consistent variants of this criterion.

Finally, we consider the following global objective function

$$J(\Omega) = \sum_{i=1}^{N_l} J_g(\Omega_i, u_\Omega^i, p_{\mathrm{mean}}), \tag{5}$$

where

$$J_g(\Omega_i, u_\Omega^i, p_{\mathrm{mean}}) = J_e(\Omega_i, u_\Omega^i) + \alpha J_p(\Omega_i, u_\Omega^i, p_{mean}), \tag{6}$$

and we study the influence of the parameter α on the optimal shape Ω.

The main contribution of this work is twofold: first of all, we propose a comparison of the penalty and Nitsche's method in the framework of shape optimization. The second contribution of this work is to propose and test an efficient criterion for the uniformization of the contact stress according to the different load positions.

In section 2, we introduce the problem with a frictional contact condition, its approximation with a penalty approach and a consistent formulation based on Nitsche's method. In section 3, the geometric shape optimization framework is presented. In section 4, we introduce the discretization used and the optimization strategy. Finally, in section 5, we present some numerical results which highlight the interest of Nitsche's method and the efficiency of the geometric shape optimization to obtain optimal domains Ω that minimize the criteria previously introduced.

2 Weak formulation of the contact problem

In this section, we describe the unilateral contact condition with friction on the boundary Γ_C and provide the weak formulation of the elastic problem for both a penalized contact condition and Nitsche's method.

2.1 Classical weak inequality formulations

The displacement $u_\Omega : \Omega \to \mathbb{R}^d$ of the body according to its reference configuration satisfies the equations of system (1). To derive a weak formulation, let us also introduce the Hilbert space $V = \{v \in H^1(\Omega; \mathbb{R}^d) : v = 0 \text{ on } \Gamma_D\}$ and the two applications $a : V \times V \to \mathbb{R}$ and $\ell : V \to \mathbb{R}$, defined for all $(u, v) \in V \times V$ by

$$a(u, v) = \int_\Omega A\varepsilon(u) : \varepsilon(v)\ \mathrm{d}x,$$

$$\ell(v) = \int_\Omega f(x) \cdot v\ \mathrm{d}x + \int_{\Gamma_N} g_N \cdot v\ \mathrm{d}s(x).$$

Then, using Green's formula and under regularity assumptions, one shows that the displacement field $u_\Omega \in V$ satisfies

$$a(u, v) - \int_{\Gamma_C} \sigma(u)n \cdot v\ \mathrm{d}s(x) = \ell(v), \quad \forall v \in V. \tag{7}$$

The obstacle is supposed to be rigid and flat. We consider n_y, the inward unit vector to the rigid obstacle and g the initial gap between the elastic body and the obstacle (see Figure 3). On the contact boundary Γ_C, the displacement $u : \Omega \to \mathbb{R}^d$, is decomposed into its normal component $u_n = u \cdot n_y$ and its tangent one $u_t = (I - n_y \otimes n_y)u$ such that

$$u = u_n n_y + u_t. \tag{8}$$

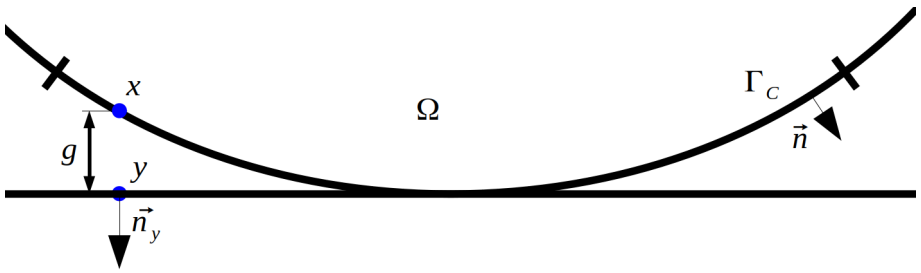

Figure 3: Contact surface representation for the vertical load configuration.

The initial gap between the body and the obstacle is defined on $x \in \Gamma_C$ by

$$g = n_y \cdot (y - x), \tag{9}$$

where y is the orthogonal projection of x upon the rigid obstacle. We note also the decomposition of the contact stress on Γ_C into normal and tangent parts:

$$\sigma_n(u) = (\sigma(u)\, n) \cdot n_y, \qquad \sigma_t(u) = (I - n_y \otimes n_y)(\sigma(u)\, n). \tag{10}$$

The unilateral contact condition on Γ_C can be expressed by the following complementary condition:

$$(u_n - g) \leq 0, \tag{11a}$$
$$\sigma_n(u) \leq 0, \tag{11b}$$
$$(u_n - g)\, \sigma_n(u) = 0. \tag{11c}$$

In case of frictionless contact, the displacement u_Ω is the minimizer of the energy $\frac{1}{2}a(u,u) - \ell(u)$ on the convex K of admissible displacements satisfying the non-interpenetration condition on the boundary Γ_C defined as

$$K := \{v \in V : v_n - g \in K_0\}, \qquad K_0 := \{v \in L^2(\Gamma_C) : v \leq 0\}. \tag{12}$$

The corresponding optimality system reads (see [21])

$$\begin{cases} \text{Find } u \in K \text{ such that} \\ a(u, v-u) \geq \ell(v-u), \qquad \forall v \in K. \end{cases} \tag{13}$$

Under standard assumptions, the existence and uniqueness of the solution to problem (13) is a direct consequence of Stampacchia's theorem.

The classical Coulomb law of friction can be written on Γ_C as

$$\begin{cases} |\sigma_t(u)| \leq -\mathcal{F}\sigma_n(u) & \text{if } \dot{u}_t = 0, \\ \sigma_t(u) \;\; = \mathcal{F}\sigma_n(u)\frac{\dot{u}_t}{|\dot{u}_t|} & \text{otherwise}, \end{cases} \tag{14}$$

where $\mathcal{F} \geq 0$ is the friction coefficient, depending on the couple of materials in contact and $\dot{u}_t$ is the sliding velocity. The Coulomb law of friction is usually approximated by replacing the sliding velocity by the finite difference

$$\frac{u_t - u_t^0}{\Delta t}, \tag{15}$$

where u_t^0 stands for the tangent displacement at an initial time step and Δt the time step. For the sake of simplicity, taking $u_t^0 = 0$ leads to the so called static Coulomb's law of friction:

$$\begin{cases} |\sigma_t(u)| \leq -\mathcal{F}\sigma_n(u) & \text{if } u_t = 0, \\ \sigma_t(u) \ = \mathcal{F}\sigma_n(u)\frac{u_t}{|u_t|} & \text{otherwise.} \end{cases} \tag{16}$$

In case of contact with friction, the displacement u_Ω is solution to the following weak inequality formulation (see [21]):

$$\begin{cases} \text{Find } u \in K \text{ such that} \\ a(u, v-u) + j(v) - j(u) \geq \ell(v-u), \quad \forall v \in K, \end{cases} \tag{17}$$

where $j(v) = -\displaystyle\int_{\Gamma_C} \mathcal{F}\sigma_n(v)|v_t|\mathrm{d}s(x)$. The existence of solutions to Problem (17) is addressed for instance in [35, 22] and is not generally ensured for arbitrary large friction coefficients. Condition of uniqueness of the solution to this problem still remains an open question, partially addressed in [47, 33, 34].

2.2 Weak formulation with a penalty method

The penalty method (see [36] for instance) is a simple way to treat contact problems. It involves an additional weak term in the weak formulation standing for a stiffness at the boundaries limiting interpenetration between the body and the obstacle. It is non-consistent in the sense that it represents a supplementary approximation of the contact condition. For $\gamma > 0$ the penalty parameter, the frictional contact conditions (11) - (16) are approximated by

$$\begin{aligned} \sigma_n(u) &= -\gamma[g - u_n]_-, \\ \sigma_t(u) &= P_{\mathcal{B}(n_y,\rho(u))}(\gamma u), \end{aligned} \tag{18}$$

where $\rho(u) = \mathcal{F}\gamma[g - u_n]_-$ is the friction threshold, the negative part being defined by $[x]_- = \frac{1}{2}(|x| - x), \forall x \in \mathbb{R}$ and the projection of an element $x \in \mathbb{R}^d$ on the ball $\mathcal{B}(n_y, \rho(u))$ of radius $\rho(u)$ on the tangent plane with respect to n_y (see also [46]) is defined by

$$P_{\mathcal{B}(n_y,\rho)}(q) = \begin{cases} (I_d - n_y \otimes n_y)q & \text{if } \ |(I_d - n_y \otimes n_y)q| \leq \rho, \\ \rho\frac{(I_d - n_y \otimes n_y)q}{|(I_d - n_y \otimes n_y)q|} & \text{otherwise.} \end{cases} \tag{19}$$

Recall that using (7) the displacement field $u_\Omega \in V$ satisfies

$$a(u, v) - \int_{\Gamma_C} (\sigma_n(u)v_n + \sigma_t(u) \cdot v_t)\mathrm{d}s(x) = \ell(v), \quad \forall v \in V. \tag{20}$$

Finally, a weak formation for the penalty method can be easily deduced by incorporating equalities (18) in (20) which conduces to introduce the solution $u_\Omega^P \in V$ of

$$a(u, v) + \mathcal{I}_P(u, v, n_y) = \ell(v), \ \forall v \in V, \tag{21}$$

where the penalty contact term $\mathcal{I}_P(u, v, n_y)$ is

$$\mathcal{I}_P(u, v, n_y) = \int_{\Gamma_C} (\gamma[g - u_n]_- \ v_n \ - P_{\mathcal{B}(n_y,\rho(u))}(\gamma u) \ \cdot \ v_t)\mathrm{d}s(x). \tag{22}$$

We refer to [21, 20] for the existence of a solution to problem (21).

2.3 Weak formulation using Nitsche's method

Nitsche's method, presented by J. Nitsche in [42], aimed first at treating Dirichlet conditions. The Nitsche method we used to account for the contact condition with friction was originally introduced in [16, 18] for frictionless contact, then generalized to Tresca's friction in [14] and Coulomb's friction in [17] (see also the overview [15]). The Nitsche method introduces a contact term which weakly prescribed the frictional contact conditions (11)-(16) in a consistent manner. It is based on the equivalent reformulation of the contact conditions which has been originally derived from the augmented Lagrangian approach [2] and reads as

$$\begin{aligned} \sigma_n(u) &= -[\sigma_n(u) - \gamma(u_n - g)]_-, \\ \sigma_t(u) &= P_{\mathcal{B}(n_y,\rho(u))}(\sigma(u)n - \gamma u), \end{aligned} \tag{23}$$

where ρ is now defined by $\rho(u) = \mathcal{F}[\sigma_n(u) - \gamma(u_n - g)]_-$. More precisely, incorporating

$$v_n = -\frac{1}{\gamma}(\theta\sigma_n(v) - \gamma v_n) + \frac{\theta}{\gamma}\sigma_n(v), \qquad v_t = -\frac{1}{\gamma}(\theta\sigma_t(v) - \gamma v_t) + \frac{\theta}{\gamma}\sigma_t(v), \tag{24}$$

for a fixed $\theta \in \mathbb{R}$ in the weak formulation (7), we see that

$$\begin{aligned} a(u,v) &- \int_{\Gamma_C} \frac{\theta}{\gamma}\sigma_n(u)\sigma_n(v)\,\mathrm{d}s(x) + \int_{\Gamma_C} \frac{1}{\gamma}\ \ \sigma_n(u)\,(\theta\,\sigma_n(v) - \gamma v_n)\,\mathrm{d}s(x) \\ &- \int_{\Gamma_C} \frac{\theta}{\gamma}\sigma_t(u)\cdot\sigma_t(v)\,\mathrm{d}s(x) + \int_{\Gamma_C} \frac{1}{\gamma}\ \ \sigma_t(u)\cdot(\theta\,\sigma_t(v) - \gamma v_t)\,\mathrm{d}s(x) = \ell(v), \quad \forall v \in V, \end{aligned} \tag{25}$$

which becomes

$$\begin{aligned} a(u,v) &- \int_{\Gamma_C} \frac{\theta}{\gamma}\sigma_n(u)\sigma_n(v)\,\mathrm{d}s(x) - \int_{\Gamma_C} \frac{1}{\gamma}\ \ [\sigma_n(u) - \gamma(u_n - g)]_-\ \ (\theta\,\sigma_n(v) - \gamma v_n)\ \ \mathrm{d}s(x) \\ &- \int_{\Gamma_C} \frac{\theta}{\gamma}\sigma_t(u)\cdot\sigma_t(v)\,\mathrm{d}s(x) + \int_{\Gamma_C} \frac{1}{\gamma}\ \ P_{\mathcal{B}(n_y,\rho(u))}(\sigma(u)n - \gamma u)\ \cdot\ (\theta\,\sigma_t(v) - \gamma v_t)\ \ \mathrm{d}s(x) \\ &= \ell(v),\ \forall\, v \in V, \end{aligned} \tag{26}$$

by using additionally (23). Finally, the Nitsche approach conduces to define the solution u_Ω^N to

$$a(u,v) + \mathcal{I}_N(u,v,n) = \ell(v),\ \forall v \in V, \tag{27}$$

where the contact term $\mathcal{I}_N(u,v,n)$ reads

$$\begin{aligned} \mathcal{I}_N(u,v,n) = \int_{\Gamma_C} (&-\frac{\theta}{\gamma}\sigma_n(u)\sigma_n(v)\,\mathrm{d}s(x) - \frac{1}{\gamma}\ \ [\sigma_n(u) - \gamma(u_n - g)]_-\,(\theta\,\sigma_n(v) - \gamma v_n) \\ &- \frac{\theta}{\gamma}\sigma_t(u)\cdot\sigma_t(v)\ + \frac{1}{\gamma}\ \ P_{\mathcal{B}(n_y,\rho(u))}(\sigma(u)n - \gamma u)\ \cdot\ (\theta\,\sigma_t(v) - \gamma v_t))\,\mathrm{d}s(x). \end{aligned} \tag{28}$$

Remark 1. *The introduction of the parameter θ leads to different variants acting on the symmetry, skew-symmetry or non-symmetry of the contact term (see [18]). In particular, in the frictionless case, when $\theta = 1$, the formulation is symmetric and admits a potential energy. When $\theta = 0$, a non-symmetric method is set whose formulation is closer to the penalty approach described in 2.2. Finally, when $\theta = -1$, the contact term is skew-symmetric and leads to interesting properties independent of the Nitsche parameter γ.*

2.4 Analysis of a Nitsche-based finite element method

Let $V^h \subset V$ be a family of finite dimensional vector spaces indexed by h coming from a family $\mathcal{T}^h$ of triangulations of the domain Ω supposed to be polygonal for the sake of simplicity ($h = \max_{T\in\mathcal{T}^h} h_T$ where h_T is the diameter of T). The family of triangulations is supposed regular (i.e., there exists $\sigma > 0$ such that $\forall T \in \mathcal{T}^h, h_T/\rho_T \leq \sigma$ where ρ_T denotes the radius of the inscribed ball in T) and conformal to the subdivision of the boundary into Γ_D, Γ_N and Γ_C (i.e. a face of an element $T \in \mathcal{T}^h$ is not allowed to have simultaneous non-empty intersection with more than one part of the subdivision). For instance, a standard Lagrange finite element method of degree k reads

$$V^h := \{v^h \in \mathscr{C}^0(\bar{\Omega})^d : v^h|_T \in (P_k(T))^d, \forall T \in \mathcal{T}^h, v^h = 0 \text{ on } \Gamma_D\}. \tag{29}$$

Let γ be a piecewise constant function on the contact interface Γ_C defined for any $x \in \Gamma_C$ lying on the relative interior of $\Gamma_C \cap T$ for a (closed) element T having a non-empty intersection of dimension $d-1$ with Γ_C by

$$\gamma(x) = \frac{\gamma_0}{h_T}, \tag{30}$$

where γ_0 is a positive given constant. The generalized Nitsche-based approximation then reads:

$$\left\{ \begin{array}{l} \text{Find } u^h \in V^h \text{ such that} \\ a(u^h, v^h) + \mathcal{I}_N(u^h, v^h, n) = \ell(v^h), \quad \forall v^h \in V^h. \end{array} \right. \tag{31}$$

The advantage of Nitsche's method over the penalty approach is its consistency which can be established in the following sense.

Lemma 2. *Suppose that the solution u of (1), (11) and (16) is in $(H^{\frac{3}{2}+\nu}(\Omega))^d$ where $d = 2, 3$ and $\nu > 0$. Then u is also solution, $\forall v^h \in V^h$, of*

$$a(u, v^h) + \mathcal{I}_N(u, v^h, n) = \ell(v^h). \tag{32}$$

Proof. Let u be the solution to (1), (11) and (16). Let v^h be in V_0^h. Since $u \in (H^{\frac{3}{2}+\nu}(\Omega))^d$ and $\nu > 0$, $\sigma_n(u)$ and $\sigma_t(u) \in H^\nu(\Gamma_C) \subset L^2(\Gamma_C)$. As a result,

$$a(u, v^h) - \int_{\Gamma_C} \frac{\theta}{\gamma}\sigma_n(u)\ \sigma_n(v^h)\ \mathrm{d}s(x) - \int_{\Gamma_C} \frac{\theta}{\gamma}\sigma_t(u)\cdot\sigma_t(v^h)\ \mathrm{d}s(x), \tag{33}$$

makes sense, and $\sigma_n(u) - \gamma(u_n - g)$ and $\sigma_t(u) - \gamma u_t \in L^2(\Gamma_C)$. Using the reformulation of $\sigma_n(u)$ and $\sigma_t(u)$ in (23) and formulation (25), it holds:

$$\begin{aligned} a(u, v^h) &- \int_{\Gamma_C} \frac{\theta}{\gamma}\sigma_n(u)\sigma_n(v^h)\ \mathrm{d}s(x) - \int_{\Gamma_C} \frac{1}{\gamma}[\sigma_n(u) - \gamma(u_n - g)]_-\ \ (\theta\sigma_n(v^h) - \gamma v_n^h)\ \mathrm{d}s(x) \\ &- \int_{\Gamma_C} \frac{\theta}{\gamma}\sigma_t(u)\cdot\sigma_t(v^h)\ \mathrm{d}s(x) + \int_{\Gamma_C} \frac{1}{\gamma}P_{\mathcal{B}(n_y,\rho(u))}(\sigma(u)n - \gamma u)\ \cdot\ (\theta\sigma_t(v^h) - \gamma v_t^h)\ \mathrm{d}s(x) \\ &= a(u, v^h) - \int_{\Gamma_C} \frac{\theta}{\gamma}\sigma_n(u)\sigma_n(v^h)\ \mathrm{d}s(x) - \int_{\Gamma_C} \frac{1}{\gamma}\sigma_n(u)\ (\theta\sigma_n(v^h) - \gamma v_n^h)\ \mathrm{d}s(x) \\ &- \int_{\Gamma_C} \frac{\theta}{\gamma}\sigma_t(u)\cdot\sigma_t(v^h)\ \mathrm{d}s(x) + \int_{\Gamma_C} \frac{1}{\gamma}\sigma_t(u)\ \cdot\ (\theta\sigma_t(v^h) - \gamma v_t^h)\ \mathrm{d}s(x) \\ &= a(u, v^h) - \int_{\Gamma_C} \sigma_n(u)v_n^h\ \mathrm{d}s(x) - \int_{\Gamma_C} \sigma_t(u)\cdot v_t^h\ \mathrm{d}s(x). \end{aligned} \tag{34}$$

In the same time, using an integration by parts, it holds:

$$a(u, v^h) - \int_{\Gamma_C} \sigma_n(u)v_n^h\ \mathrm{d}s(x) - \int_{\Gamma_C} \sigma_t(u)\cdot v_t^h\ \mathrm{d}s(x) = \ell(v^h), \tag{35}$$

which ends the proof, as the equality is strictly respected, whatever θ is. □

The well-posedness and the consistency are analyzed in [16] and [18] for the frictionless formulation. When $\theta = -1$, the well-posedness does not depend on γ_0 anymore, which implies that the value of $\theta = -1$ is a convenient choice for the rest of the computation if robustness is required. Concerning the Nitsche-based formulation with the Coulomb law of friction, the existence of solution is studied in [17].

3 Geometric shape optimization

The geometric shape optimization aims at minimizing a criterion $J(\Omega)$ to find the optimal shape of a structure by forcing the domain frontiers to evolve. The energy of the structure can be expressed as a target criterion. If several criteria must be minimized, that energy can be a combination of these criteria and lead to a multi-criterion optimization. The generic formulation for the energy or the target criterion might be expressed as

$$J(\Omega) = \int_\Omega \mathcal{M}(u_\Omega, x)\, \mathrm{d}x + \int_{\partial\Omega} \mathcal{N}(u_\Omega, x)\, \mathrm{d}s(x), \tag{36}$$

where u_Ω is defined as the solution of

$$a(u_\Omega, v) + \mathcal{I}(u_\Omega, v, n) = \ell(v),\ \forall v \in V.$$

Here the contact term $\mathcal{I}$ is written as $\mathcal{I}(u, v, n) = \mathcal{I}_P(u, v, n)$ or $\mathcal{I}(u, v, n) = \mathcal{I}_N(u, v, n)$ according to the contact approximation used. Here, $\mathcal{M}$ and $\mathcal{N}$ are two functions assumed to be sufficiently smooth so that the shape derivative of J is well defined.

Remark 3. *As specified for instance in [38], it is often assumed that*

$$\begin{aligned} |\mathcal{M}(u,x)| &\le C(1+|u|^2), & |\mathcal{N}(u,x)| &\le C(1+|u|^2), \\ |\langle \mathcal{D}_u\, \mathcal{M}(u,x), v\rangle| &\le C|u\cdot v|, & |\langle \mathcal{D}_u\, \mathcal{N}(u,x), v\rangle| &\le C|u\cdot v|, \end{aligned} \tag{37}$$

for some constants $C > 0$ which includes the case of the compliance energy when it is expressed as

$$J(\Omega) = \int_\Omega f u_\Omega\, \mathrm{d}x + \int_{\Gamma_N} g_N \cdot u_\Omega\, \mathrm{d}s(x).$$

Yet using additional frictional contact terms, it is not clear whether this expression takes properly into account the elastic strain energy or not and we prefer to use the following formulation

$$J(\Omega) = \int_\Omega \frac{1}{2} A\varepsilon(u_\Omega) : \varepsilon(u_\Omega)\mathrm{d}x,$$

which unfortunately does not meet the above conditions. However, as we will see later, these conditions are not necessary to obtain the existence of the shape derivatives of the criteria we use.

Let $\mathcal{D} \subset \mathbb{R}^d$ be a fixed bounded and smooth domain whose boundary is split into Γ_C and Γ_D supposed in our case to be some fixed non-optimizable boundaries. Let Ω_{ad} be the admissible set composed of all smooth open domains Ω having Γ_C and Γ_D as parts of its boundary and having an additional optimizable boundary Γ_N (see Figure 1)

$$\Omega_{ad} := \{\Omega \subset \mathcal{D} | \Omega \text{ open and of class } \mathscr{C}^1, \Gamma_C \subset \overline{\Omega}, \Gamma_D \subset \overline{\Omega}\}. \tag{38}$$

Then, the shape optimization consists in finding some domains $\Omega \in \Omega_{ad}$ minimizing the target criterion $J(\Omega)$ with a volume constraint.

Note that, in the rest of the paper, we use the following notation of the directional derivative of an element A with respect to x in the direction y:

$$\langle \mathcal{D}_x\, A(x), y\rangle = \lim_{\epsilon\to 0} \frac{A(x+\epsilon y) - A(x)}{\epsilon}. \tag{39}$$

3.1 Shape derivative

The differentiation with respect to the domain aims at modifying the reference state of the domain $\Omega \in \Omega_{ad}$ using the boundary method first described by J. Hadamard in [24] and then developed for instance in [32], [41], [45], [50] and [52]. Let $\Theta \in W^{1,\infty}(\mathbb{R}^d;\mathbb{R}^d) \cap \mathscr{C}^1(\mathbb{R}^d)$ be a vector field displacing the reference domain Ω towards different admissible shapes $\Omega_t \in \Omega_{ad}$. The domain variation in the direction $t\Theta$ reads for t small:

$$\Omega_t = (Id + t\Theta)(\Omega). \tag{40}$$

The shape derivative $\langle \mathcal{D}\, J(\Omega), \Theta\rangle$ of $J(\Omega)$ with respect to the reference domain Ω in the direction Θ is defined as the derivative on $t = 0$ of the application $t \mapsto J(\Omega_t)$ when it exists and gives

$$J(\Omega_t) = J(\Omega) + t\, \langle \mathcal{D}\, J(\Omega), \Theta\rangle + o(t). \tag{41}$$

Recall that the shape gradient for general functional in a context of linear elasticity with penalized contact is derived in [38]. We develop the case where Nitsche's method is used to deal with the contact although the contact boundary Γ_C is not optimized.

Theorem 4. *Assume that $f \in H^1(\Omega;\mathbb{R})$, $g \in H^2(\Omega;\mathbb{R})$ and that (21) or (27) admits a unique solution $u_{\Omega_t} \in H^1(\Omega_t;\mathbb{R})$ for t small enough and $\Theta \in W^{1,\infty}(\mathbb{R}^d;\mathbb{R}^d)$. If we denote $\langle \mathcal{D}\, J(\Omega), \Theta\rangle$ the Gâteaux derivative of $J(\Omega)$ with respect to Ω in the direction $\Theta \in W^{1,\infty}(\mathbb{R}^d;\mathbb{R}^d)$, we have when this derivative exists:*

$$\begin{aligned}\langle \mathcal{D}\, J(\Omega), \Theta\rangle \;=\; & \int_{\Gamma_m} (\Theta\cdot n)\,(\mathcal{M}(u_\Omega, x) + A\varepsilon(u_\Omega) : \varepsilon(p_\Omega) - f(x)\cdot p_\Omega)\,\mathrm{d}s(x) \\ & + \int_{\Gamma_m} (\Theta\cdot n)\,(\kappa_m\, \mathcal{N}(u_\Omega, x) + \nabla \mathcal{N}(u_\Omega, x)\cdot n)\,\mathrm{d}s(x) \\ & - \int_{\Gamma_m\cap\Gamma_N} (\Theta\cdot n)\,(\kappa_m\, p_\Omega\cdot g_N + \nabla(p_\Omega\cdot g_N)\cdot n)\,\mathrm{d}s(x).\end{aligned} \tag{42}$$

where Γ_m is a moving boundary of Ω, assuming $\Gamma_m \cap \Gamma_C = \Gamma_m \cap \Gamma_D = \emptyset$, κ_m is the mean curvature of $\partial\Omega$, and p_Ω is the adjoint state defined as the solution of

$$a(q,p) + \langle \mathcal{D}_u\, \mathcal{I}(u_\Omega, p, n), q\rangle + \int_\Omega \langle \mathcal{D}_u\, \mathcal{M}(u_\Omega, x), q\rangle \mathrm{d}x + \int_{\partial\Omega} \langle \mathcal{D}_u\, \mathcal{N}(u_\Omega, x), q\rangle \mathrm{d}s(x) = 0,\ \forall q \in V. \tag{43}$$

Remark 5. *As explained previously, the existence of adjoint state problem requires that the applications $q \mapsto \langle \mathcal{D}_u\, \mathcal{M}(u_\Omega, x), q\rangle$ and $q \mapsto \langle \mathcal{D}_u\, \mathcal{N}(u_\Omega, x), q\rangle$ must be continuous in V, which is clearly the case under assumptions (37). However, these conditions are sufficient but not necessary to verify these continuity properties.*

We develop now the Lagrangian method introduced by J. Céa [11] which aims at describing a constrained optimization problem. To this end, we first present two useful results: let Ω be a bounded open and regular set from $\mathbb{R}^d$.

- Let $f \in H^1(\Omega, \mathbb{R})$ and let the application $J : \Omega_{\mathrm{ad}} \mapsto \mathbb{R}$ defined by

$$J(\Omega) = \int_\Omega f(x)\,\mathrm{d}x. \tag{44}$$

  Then J is differential with respect to Ω in the direction $\Theta \in \mathscr{C}^1(\mathbb{R}^d, \mathbb{R}^d)$ and

$$\langle \mathcal{D}\, J(\Omega), \Theta\rangle = \int_{\partial\Omega} \Theta\cdot n\, f(x)\,\mathrm{d}s(x). \tag{45}$$

- Let $g \in H^1(\Omega, \mathbb{R})$ and let the application $J : \Omega_{\text{ad}} \mapsto \mathbb{R}$ defined by

$$J(\Omega) = \int_{\partial\Omega} g \, \mathrm{d}s(x). \tag{46}$$

Then J is differential in Ω and for all $\Theta \in \mathscr{C}^1(\mathbb{R}^d \, \mathbb{R}^d)$ and

$$\langle \mathcal{D} \, J(\Omega), \Theta \rangle = \int_{\partial\Omega} \Theta \cdot n \, (\nabla g(x) \cdot n + \kappa_m g(x)) \, \mathrm{d}s(x). \tag{47}$$

Proof of theorem (4)*:*
We intend to minimize the criterion $J(\Omega)$ given by (36) under the constraint that the weak formulation (21) or (27) is satisfied. Let $\mathcal{L} : V \mapsto \mathbb{R}$, the Lagrangian application defined by

$$\mathcal{L}(u, v, n, \Omega) = J(\Omega, u) + (a(u, v) + \mathcal{I}(u, v, n) - \ell(v)). \tag{48}$$

where $J(\Omega, u) = \displaystyle\int_\Omega \mathcal{M}(u, x) \, \mathrm{d}x + \int_{\partial\Omega} \mathcal{N}(u, x) \, \mathrm{d}s(x)$. The key is to remark that $J(\Omega) = J(\Omega, u_\Omega)$ and then to identify $J(\Omega)$ as

$$J(\Omega) = \mathcal{L}(u_\Omega, v, n, \Omega). \tag{49}$$

If $\mathcal{L}$ is differentiated with respect to the domain Ω in the direction Θ, it gives

$$\begin{aligned} \langle \mathcal{D} \, J(\Omega), \Theta \rangle &= \langle \mathcal{D} \left[\mathcal{L}(u_\Omega, v, n, \Omega) \right], \Theta \rangle \\ &= \langle \mathcal{D}_\Omega \, \mathcal{L}(u_\Omega, v, n, \Omega), \Theta \cdot n \rangle + \langle \mathcal{D}_n \, \mathcal{L}(u_\Omega, v, n, \Omega), \langle \mathcal{D}_\Omega \, n, \Theta \rangle \rangle \\ &+ \langle \mathcal{D}_u \, \mathcal{L}(u_\Omega, v, n, \Omega), \langle \mathcal{D}_\Omega \, u_\Omega, \Theta \rangle \rangle. \end{aligned} \tag{50}$$

In order to vanish the last term of equation (50) and obtain an explicit formulation of the shape derivative of J, the idea is to follow the method of the adjoint state introduced by J.-L. Lions in [37]. More precisely, let $p_\Omega \in V$ be defined as the solution of

$$\langle \mathcal{D}_u \, \mathcal{L}(u_\Omega, p_\Omega, n, \Omega), q \rangle \; = 0, \; \forall q \in V. \tag{51}$$

Then, evaluating the equation (50) at $v = p_\Omega$ shows that

$$\langle \mathcal{D}_\Omega \, \mathcal{L}(u_\Omega, p_\Omega, n, \Omega), \Theta \rangle \; = \; \langle \mathcal{D}_\Omega \, \mathcal{L}(u_\Omega, p_\Omega, n, \Omega), \Theta \cdot n \rangle + \langle \mathcal{D}_n \, \mathcal{L}(u_\Omega, p_\Omega, n, \Omega), \langle \mathcal{D}_\Omega \, n, \Theta \rangle \rangle, \tag{52}$$

as $\langle \mathcal{D}_\Omega \, u, \Theta \rangle \in V$. Moreover, the term $\langle \mathcal{D}_u \, \mathcal{L}(u, p, n, \Omega), q \rangle$ can be identified as

$$\begin{aligned} \langle \mathcal{D}_u \, \mathcal{L}(u, p, n, \Omega), q \rangle &= a(q, p) + \langle \mathcal{D}_u \, \mathcal{I}(u, p, n), q \rangle \\ &+ \int_\Omega \langle \mathcal{D}_u \, \mathcal{M}(u, x), q \rangle \, \mathrm{d}x + \int_{\partial\Omega} \langle \mathcal{D}_u \, \mathcal{N}(u, x), q \rangle \, \mathrm{d}s(x). \end{aligned} \tag{53}$$

This leads to the following explicit expression of the shape gradient in linear elasticity:

$$\begin{aligned} \langle \mathcal{D} \, J(\Omega), \Theta \rangle \; &= \; \int_{\Gamma_m} (\Theta \cdot n) \, (\mathcal{M}(u_\Omega, x) + A\varepsilon(u_\Omega) : \varepsilon(p_\Omega) - f(x) \cdot p_\Omega) \, \mathrm{d}s(x) \\ &+ \int_{\Gamma_m} (\Theta \cdot n) \, (\kappa_m \, \mathcal{N}(u_\Omega, x) + \nabla \mathcal{N}(u_\Omega, x) \cdot n) \, \mathrm{d}s(x) \\ &- \int_{\Gamma_m \cap \Gamma_N} (\Theta \cdot n) \, (\kappa_m \, p_\Omega \cdot g_N + \nabla (p_\Omega \cdot g_N) \cdot n) \, \mathrm{d}s(x), \end{aligned} \tag{54}$$

as $\Gamma_m \cap \Gamma_C = \emptyset$ and $\mathcal{I}(u, p, n)$ is an integral term defined on Γ_C.

□

3.2 Contact term

In this section, we give an explicit formulation of the contact term and its directional derivative in the adjoint equation.

3.2.1 Case of the penalty method

In this case, we have $\mathcal{I}(u,v,n) = \mathcal{I}_P(u,v,n)$ defined by (22). The derivative term $\langle \mathcal{D}_u \mathcal{I}_P(u,p,n), q\rangle$ from (43) can then be developed as

$$\langle \mathcal{D}_u \mathcal{I}_P(u,p,n), q\rangle = -\int_{\Gamma_C} \left(\gamma\, H(-(g-u_n))q_n\, p_n + \mathcal{D}_u\, P_{\mathcal{B}(n_y,\rho(u))}(\gamma u)\, \gamma q_t \cdot p_t\right) \mathrm{d}s(x), \tag{55}$$

where H is the Heaviside function defined by $H(x) = 1$ for $x \geq 0$ and $H(x) = 0$ otherwise. Moreover, the computation of $\mathcal{D}_u\, P_{\mathcal{B}(n,\rho(u))}((\gamma u))$ is obtained thanks to the the partial derivatives of the projection ball $P_{\mathcal{B}(n,\tau)}(q)$ according to q and τ. Indeed, it reads (see [46])

$$\partial_q P_{\mathcal{B}(n,\tau)}(q) = \begin{cases} 0 & \text{for } \tau \leq 0, \\ T_n & \text{if } |q_t| \leq \tau, \\ \frac{\tau}{|q_t|}(T_n - \frac{q_t}{|q_t|} \otimes \frac{q_t}{|q_t|}) & \text{otherwise,} \end{cases} \tag{56}$$

and

$$\partial_\tau P_{\mathcal{B}(n,\tau)}(q) = \begin{cases} 0 & \text{for } \tau \leq 0 \text{ or } |q_t| \leq \tau, \\ \frac{q_t}{|q_t|} & \text{otherwise,} \end{cases} \tag{57}$$

Where T_n is defined by $T_n = I_d - n \otimes n$, $q_t = T_n q$. We refer to [12] for the differentiability of the penalty approach.

3.2.2 Case of Nitsche's approach

Concerning Nitsche's method, we now have $\mathcal{I}(u,v,n) = \mathcal{I}_N(u,v,n)$ defined by (28).

The directional derivative $\langle \mathcal{D}_u \mathcal{I}_\mathcal{N}(u,p,n), q\rangle$ from (43) has the following form

$$\begin{aligned} \langle \mathcal{D}_u \mathcal{I}_N(u,p,n), q\rangle = \int_{\Gamma_C} & (-\frac{\theta}{\gamma}\sigma_n(q)\sigma_n(p) \ -\frac{\theta}{\gamma}\sigma_t(q)\cdot\sigma_t(p) \\ & + \ \frac{1}{\gamma}\, H(-(\sigma_n(u) - \gamma(u_n - g)))(\sigma_n(q) - \gamma q_n)\, (\theta\, \sigma_n(p) - \gamma p_n) \\ & + \ \frac{1}{\gamma}\, \mathcal{D}_u\, P_{\mathcal{B}(n_y,\rho(u))}(\sigma(u)n - \gamma u)(\sigma_t(q) - \gamma q_t)\cdot(\theta\, \sigma_t(p) - \gamma p_t))\, \mathrm{d}s(x). \end{aligned} \tag{58}$$

Remark 6. *Note that the term $\langle \mathcal{D}_u \mathcal{I}_N(u,p,n), q\rangle$ is not clearly defined in the continuous framework because of the possible lack of regularity of u_Ω and p_Ω. In this work, we focus only on the discrete case which does not pose any existence problem. The analysis of the convergence of the solutions of the discrete problem will be addressed in a further work.*

3.3 Criterion minimization

The main energy that is to be minimized, namely the elastic strain energy and defined by (3) can then be expressed in the general form (36) by considering

$$\mathcal{M}(u^i_\Omega, x) = \frac{1}{2} A\varepsilon(u^i_\Omega) : \varepsilon(u^i_\Omega) \text{ and } \mathcal{N}(u^i_\Omega, x) = 0.$$

Consequently, the associated term in the adjoint equation of the strain energy criterion (3) reads

$$\langle \mathcal{D}_u J_e(\Omega, u_\Omega), q\rangle = \int_\Omega A\varepsilon(q) : \varepsilon(u_\Omega)\, \mathrm{d}x. \tag{59}$$

Note that a sufficient condition for the adjoint equation to make sense is that $q \mapsto \langle \mathcal{D}_u J_e(\Omega, u_\Omega), q\rangle$ is continuous in V which is satisfied here even though the term do not meet the conditions (37).

An additional criterion developed in this work consists of uniformizing the contact stress on the contact boundary of the rolling structure according to the load positions. As mentioned in the introduction, a first natural idea would be to minimize the objective function (4). However, this expression is possibly difficult to define according to the regularity of u^i_Ω whose basic guaranteed regularity is to be in $H^1(\Omega, \mathbb{R}^d)$. Assuming additionally a square integrable right hand side, the trace $\sigma(u_\Omega)n$ on Γ_C belongs only to $H^{-1/2}(\Gamma_C, \mathbb{R}^d)$ (see [36]) and not necessarily to $L^2(\Gamma_C, \mathbb{R})$ meaning in particular that there is no continuous dependence of the objective function (4) with respect to the data of the problem.

Two variants of the criterion will be developed to recover this continuity. A first idea is to thicken the contact boundary of a size ϵ , which leads to the first criterion

$$J_{p,1}(\Omega, u_\Omega, p_{mean}) = \int_{\Gamma^\epsilon_C} \frac{L}{2E\epsilon}(\sigma(u_\Omega)n - p_{mean})^2 \mathrm{d}x, \tag{60}$$

where $\epsilon > 0$ is a fixed small length, Γ^ϵ_C is an annulus delimited by Γ_C on the exterior and of thickness ϵ and n is an extension in the domain Γ^ϵ_C of the unit outward normal vector on Γ_C. A second idea is to consider a criterion depending on the $H^{-1/2}(\Gamma_C, \mathbb{R}^d)-$norm by considering the energy

$$J_{p,2}(\Omega, u_\Omega, p_{mean}) = \frac{1}{2}\|\sigma(u_\Omega)n - p_{mean}\|^2_{H^{-1/2}(\Gamma_C, \mathbb{R}^d)}. \tag{61}$$

In order to simplify the minimization of $J_{p,1}$ and $J_{p,2}$, we treat the computation of p_{mean} by freezing it to the value at the previous optimization step. The advantage of that is to uncouple the computation of the adjoint problem on each load position.

3.3.1 Uniformity of the contact stress on the thickened boundary

As explained previously, a first strategy consists in thickening the contact boundary with a size ϵ which leads to the criterion (60). It can be expressed in the general form (36) with

$$\mathcal{M}(u_\Omega, x) = \frac{L}{2E\epsilon}(\sigma(u_\Omega)n - p_{mean})^2\, \chi_{\Gamma^\epsilon_C}(x), \quad \text{and} \quad \mathcal{N}(u_\Omega, x) = 0, \tag{62}$$

where $\chi_{\Gamma^\epsilon_C}(x) = \begin{cases} 1 & \text{if } x \in \Gamma^\epsilon_C, \\ 0 & \text{otherwise} \end{cases}$. In that case, the associated term in the adjoint equation of the contact stress criterion from equation (60), assuming p_{mean} known in advance, reads as

$$\langle \mathcal{D}_u J_{p,1}(\Omega, u_\Omega, p_{mean}), q\rangle = \int_{\Gamma^\epsilon_C} \frac{L}{E\epsilon}(\sigma(u_\Omega)n - p_{mean}) \cdot \sigma(q)n\, \mathrm{d}x. \tag{63}$$

Note that in this case, $q \mapsto \langle \mathcal{D}_u J_{p,1}(\Omega, u_\Omega, p_{mean}), q\rangle$ is continuous on V.

3.3.2 Uniformity of contact stress using a $H^{-1/2}(\Gamma_C, \mathbb{R}^d)-$norm

The second strategy consists in minimizing the functional (61). It can be expressed constructively using a Neumann to Dirichlet operator (see for instance [47] and [1]). Indeed, let $\mathcal{B}$ be a fixed domain whose

boundary is decomposed as the union of Γ_C and Γ_D. We first introduce the norm $||\cdot||_{H_{00}^{1/2}(\Gamma_C,\mathbb{R}^d)}$ defined by

$$||w||_{H_{00}^{1/2}(\Gamma_C,\mathbb{R}^d)} = \inf_{z\in V_0, z=w \text{ on } \Gamma_C} ||z||_{V_0}, \tag{64}$$

where $V_0 = \{v \in H^1(\mathcal{B};\mathbb{R}^d), v = 0 \text{ on } \Gamma_D\}$ and

$$||z||_{V_0}^2 = \int_{\mathcal{B}} A\,\varepsilon(z) : \varepsilon(z)\,\mathrm{d}x. \tag{65}$$

The norm $||\cdot||_{H^{-1/2}(\Gamma_C,\mathbb{R}^d)}$ is then defined as the dual of $||\cdot||_{H_{00}^{1/2}(\Gamma_C,\mathbb{R})}$ by

$$||g||_{H^{-1/2}(\Gamma_C,\mathbb{R}^d)} = \sup_{z\in H_{00}^{1/2}(\Gamma_C,\mathbb{R}), z\neq 0} \frac{\langle g, z\rangle}{||z||_{H_{00}^{1/2}(\Gamma_C,\mathbb{R})}} = \sup_{z\in V_0} \frac{\langle g, z\rangle}{||z||_{V_0}}. \tag{66}$$

In particular, we can show that

$$||g||_{H^{-1/2}(\Gamma_C,\mathbb{R}^d)} = ||w[g]||_{V_0}, \tag{67}$$

where $w[g] \in V_0$ is defined as the solution of

$$\begin{cases} \text{- div } \sigma(w) = 0 & \text{in } \mathcal{B} \text{ where } \sigma(w) = A\,\varepsilon(w), \\ \sigma(w)n \ = g & \text{on } \Gamma_C, \\ w \ = 0 & \text{on } \Gamma_D. \end{cases} \tag{68}$$

The weak formulation of (68) reads as

$$\int_{\mathcal{B}} A\,\varepsilon(w[g]) : \varepsilon(z)\,\mathrm{d}x = \langle g, z\rangle, \forall z \in V_0, \tag{69}$$

which shows also by using $z = \omega[g]$ that $\omega[g]$ satisfies

$$\frac{1}{2}\int_{\mathcal{B}} A\varepsilon(\omega[g]) : \varepsilon(\omega[g])\,\mathrm{d}x = \langle g, \omega[g]\rangle = \int_{\Gamma_C} g\cdot\omega[g] ds(x). \tag{70}$$

Using these equalities, the criterion for the uniformization of the contact stress finally reads

$$\begin{aligned} J_{p,2}(\Omega, u_\Omega, p_{mean}) &= \frac{1}{2}\|\sigma(u_\Omega)n - p_{mean}\|^2_{H^{-1/2}(\Gamma_C,\mathbb{R}^d)} = \frac{1}{2}\|w_\Omega\|^2_{V_0} \\ &= \frac{1}{2}\int_{\mathcal{B}} \sigma(w_\Omega) : \varepsilon(w_\Omega)\,\mathrm{d}x = \frac{1}{2}\int_{\Gamma_C} g\cdot w_\Omega\,\mathrm{d}s(x) \\ &= \frac{1}{2}\int_{\Gamma_C} (\sigma(u_\Omega)n - p_{mean})\cdot w_\Omega\,\mathrm{d}s(x). \end{aligned} \tag{71}$$

where $w_\Omega = \omega[\sigma(u_\Omega)n - p_{mean}]$ is the solution to (68) for $g = \sigma(u_\Omega)n - p_{mean}$.

Still assuming p_{mean} known in advance, the associated term in the adjoint equation of the $H^{-1/2}(\Gamma_C,\mathbb{R}^d)-$norm criterion reads

$$\begin{aligned} \langle \mathcal{D}_u\, J_{p,2}(\Omega, u_\Omega, p_{mean}), q\rangle &= \frac{1}{2}\int_\Omega \langle \mathcal{D}_u\, A\varepsilon(w_\Omega)^2, q\rangle\,\mathrm{d}x = \int_\Omega A\varepsilon(w_\Omega) : \varepsilon(w[\sigma(q)n]))\,\mathrm{d}x \\ &= \int_{\Gamma_C} \sigma(q)n\cdot w_\Omega\ \mathrm{d}s(x), \end{aligned} \tag{72}$$

where $w[\sigma(q)n]$ is defined as the solution to (68) for $g = \sigma(q)n$. As previously, the existence of the adjoint would expect the continuity of $q \mapsto \langle \mathcal{D}_u\, J_{p,2}(\Omega, u_\Omega, p_{mean}), q\rangle$ in V which is not satisfied but is the case in a subspace $H_\sigma = \{v \in V : \mathrm{div}(\sigma(v)) \in L^2(\Omega)\}$ containing the solutions of the contact problem.

Remark 7. *The Dirichlet to Neumann operator can also be defined by an intermediary Poisson problem instead of the elasticity problem* (68)*. The preference given here to the elasticity problem is guided by mechanical considerations.*

4 Numerical discretization and optimization strategy

The aim of this section is to introduce the optimization strategy to minimize the objective function given by (5) and (6). Since the optimization is to be performed on the whole structure, it would be necessary to make computations for all the load positions. In order to save some computational time, we assume a certain periodicity of the structure, using its axi-symmetry, and we perform computations only for the load positions corresponding to a single sector of the structure. The structure is divided into $N_s = 16$ sectors (see Figure 4) and we perform the computations on N_d load positions corresponding to only one sector, regularly spaced in rotations of angles $i2\pi/(N_d \times N_s)$ for i from 1 to N_d. Then the computations for the load positions corresponding to the other sectors are deduced by a simple rotation, so that we obtain at the end the computations for $N_l = N_d \times N_s$ load positions.

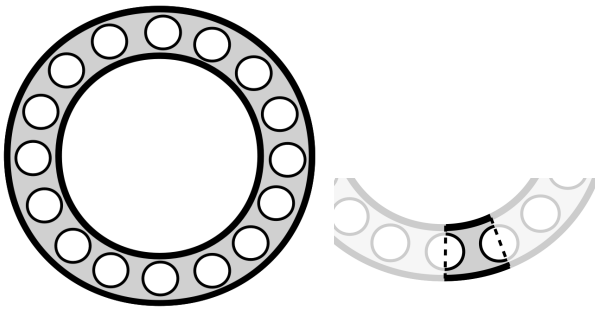

Figure 4: Periodicity of the domain Ω. On the left: the domain drilled by 16 circular holes and on the right: focus on the sector corresponding to the load positions for which computations are performed.

We consider a minimizing sequence Ω^k of J starting from an initial domain Ω^0 and taking volume and symmetry constraints into account. From a domain Ω^k, we intend to reach a domain Ω^{k+1} by performing the following steps:

- For each load position on the first sector, for i from 1 to N_d, we compute $u^i_{\Omega^k}$ the solution to the direct non-linear problem (21) or (27) approximated by a finite element method. The solutions $u^i_{\Omega^k}$ for i from $N_d + 1$ to $N_d \times N_s$ are deduced by rotations of solutions on the first sector.
- The mean contact stress p^k_{mean} is computed on Γ_C:

$$p^k_{mean} = \frac{1}{N_d} \sum_i^{N_d} (\sigma(u^i_{\Omega^k})n). \tag{73}$$

- For each load position on the first sector, for i from 1 to N_d, we compute $p^i_{\Omega^k}$ the solution to the adjoint problem (51) approximated by a finite element method. The solutions $p^i_{\Omega^k}$ for i from $N_d + 1$ to $N_d \times N_s$ are also deduced by rotations of solutions on the first sector.
- For each load position, we compute the shape gradient of $J_g(\Omega^k, u^i_{\Omega^k})$ which we extend harmonically into the holes by solving a Poisson equation.
- We sum each term to obtain the shape gradient $\overline{G^k} = \nabla J(\Omega^k)$ of $J(\Omega^k)$ on all the load positions.
- We prescribe the volume to remain constant thanks to a penalization on the gradient as $\tilde{G}^k = G^k - \lambda_k$ where $\lambda_k = 8 * (\max(G^k) - \min(G^k)) * (r^0_v - r^k_v)$ is the Lagrange multiplier with r^k_v the volume ratio at iteration k.
- We compute the new shape Ω^{k+1} by approximating the equation $\Omega^{k+1} = (I_d - \delta_k \tilde{G}^k)(\Omega^k)$, δ_k being the descent step of the shape optimization.

As an illustration, Figure 5 successively depicts the treatments led on the shape gradients: The computation of the shape gradient on a load position, the harmonic extension of that shape gradient, and the summed gradients, periodically repeated on the different sectors and the additional correction for volume constraint.

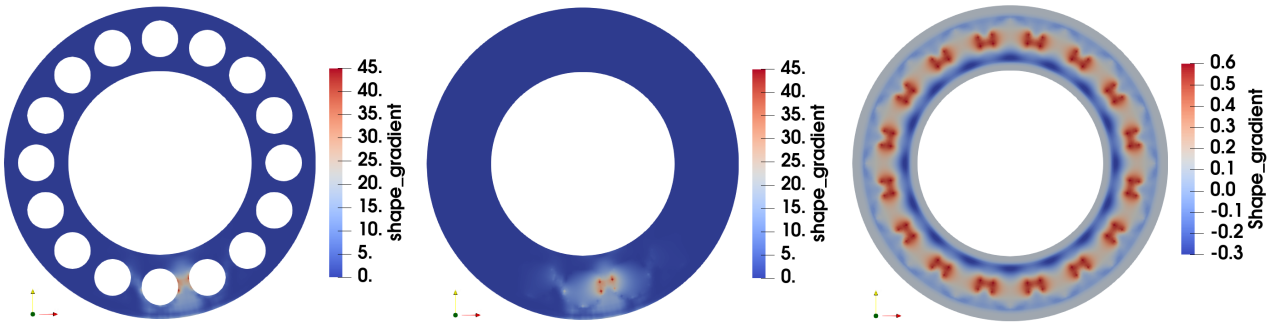

Figure 5: Successive shape gradient treatments. Left to right: the shape gradient computed on the cut elements from the solutions u_{Ω^k} and p_{Ω^k}, the harmonic extension of the shape gradient on the complete mesh and the symmetry and volume correction of the shape gradient.

4.1 Domain representation and level set function

The level set method has been introduced by S. J. Osher and J. A. Sethian in [43] to describe a geometry and its evolutions. The first applications of the level set method were about geodesics, lithography, generation of minimal surfaces, propagation of flame fronts and fluid interfaces. This method was first introduced for shape optimization applications by S. J. Osher and F. Santosa in [44] and then by G. Allaire et al. in [3] and [4]. Let $\mathcal{D} \subset \mathbb{R}^d$ still being a fixed bounded domain in which the domain Ω is included. The representation of the domain Ω in $\mathcal{D}$ is expressed by a function ψ defined in $\mathcal{D}$ as:

$$\begin{cases} \psi(x) = 0 \text{ if } x \in \partial\Omega, \\ \psi(x) < 0 \text{ if } x \in \Omega, \\ \psi(x) > 0 \text{ otherwise.} \end{cases} \tag{74}$$

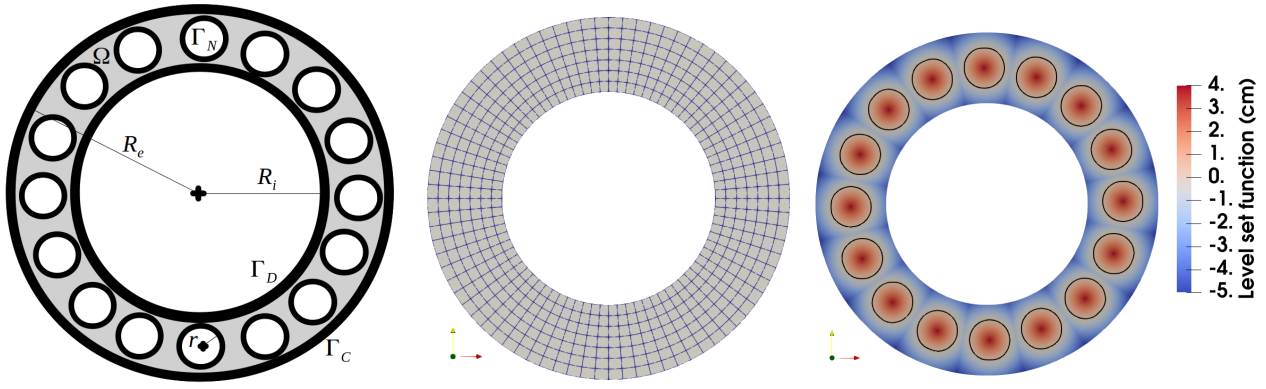

Figure 6: Representation of the domain Ω. Left to right: a schematic representation of the domain, a regular polar grid to approximate the level set and the level set representation of the domain.

The interface between holes and matter is represented by the zero value of the level set function. One way to represent the level set function ψ is to define the latter as a signed distance function

according to the domain boundaries:

$$\psi(x) = \begin{cases} -d(x, \partial\Omega) & \text{if } x \in \Omega, \\ d(x, \partial\Omega) & \text{otherwise,} \end{cases} \tag{75}$$

where $d(x, \partial\Omega)$ is the distance between x and $\partial\Omega$.

The particular situation we use for our application, i.e. the representation of a load-bearing rolling structure is depicted in Figure 6. The domain $\mathcal{D}$ is a ring of minor radius R_i and of major radius R_e. In our main numerical tests, we consider sixteen holes in the initial domain Ω^0. The optimization process only takes place at the interface of the different holes.

4.2 Transport and redistancing

For each step, the domain Ω^k is represented by the function ψ^k. A crucial step consists of transporting the level set function ψ^k by the perturbed shape gradient G^k by solving the transport equation

$$\begin{cases} \partial_t \varphi(t,x) & = -\tilde{G}^k \, |\nabla \varphi(t,x)|, \\ \varphi(0,x) & = \psi^k(x), \end{cases}$$

and taking $\psi^{k+1}(x) = \varphi(\delta_k, x)$, where δ_k is the descent step in the shape gradient algorithm.

For reason of efficiency and simplicity, the numerical approximation of this transport step is performed using Sethian's finite difference schemes (see [49]) with a slight adaptation for the polar grid.

As it is well known, successive transport steps applied to the level-set function can degrade its properties and in particular move it away from a signed distance. To remedy this, we classically apply some reinitialization steps (see for instance [53]), also based on Sethian's schemes.

Additionally, to avoid irregularities brought by the level set transport, some smoothing steps are also added consisting in finding the minimum of

$$E(\psi) = \int_\Omega \frac{1}{2}(\psi(x) - \psi^{k+1}(x))^2 \mathrm{d}x + \int_\Omega \frac{\tau}{2} |\nabla \psi(x)|^2 \mathrm{d}x, \tag{76}$$

as developed for instance in [19]. The smoothing parameter τ must be wisely set to smooth the solution without disrupting it.

4.3 Load condition on a rigid rim

Aiming at a model closer to a load-bearing rolling structure, the Dirichlet condition on Γ_D is replaced by a rigid boundary condition (rim) that is only allowed to have a vertical rigid motion and is subject to a global load. Denoting g_D the prescribed load and α_D the unknown vertical rigid displacement on Γ_D, the weak formulation reads now

$$\begin{cases} \text{Find } u \in V, \alpha_D \in \mathbb{R}, \lambda_D \in H^{-1/2}(\Gamma_D)^d \text{ such that } \forall v \in V, \forall \beta_D \in \mathbb{R} \text{ and } \forall \mu_D \in H^{-1/2}(\Gamma_D)^d, \\ a(u,v) + \mathcal{I}(u,v,n) = \displaystyle\int_\Omega f(x) \cdot v \, \mathrm{d}x + \int_{\Gamma_D} (\lambda_D \cdot v + (u - \alpha_D n_y) \cdot \mu_D + (\lambda_D \cdot n_y - g_D)\beta_D) \, \mathrm{d}s(x). \end{cases} \tag{77}$$

where λ_D is a multiplier representing the force density on Γ_D introduced to enforce the condition.

Consequently, a new term is added to the adjoint problem on Γ_D and the two new variables α_D and λ_D are introduced in the Lagrangian. The adjoint problem now reads $\forall q \in V, \forall q_{\alpha_D} \in \mathbb{R}$ and $\forall q_{\lambda_D} \in H^{-1/2}(\Gamma_D)^d$,

$$\begin{aligned} \langle \mathcal{D}_u \mathcal{L}(u,p,\alpha_D,\lambda_D,n,\Omega), q \rangle + \langle \mathcal{D}_{\alpha_D} \mathcal{L}(u,p,\alpha_D,\lambda_D,n,\Omega), q_{\alpha_D} \rangle \\ + \langle \mathcal{D}_{\lambda_D} \mathcal{L}(u,p,\alpha_D,\lambda_D,n,\Omega), q_{\lambda_D} \rangle = 0, \end{aligned} \tag{78}$$

which leads to

$$\begin{cases} \text{Find } p \in V, p_{\alpha_D} \in \mathbb{R}, p_{\lambda_D} \in H^{-1/2}(\Gamma_D)^d \text{ such that } \forall q \in V, \forall q_{\alpha_D} \in \mathbb{R} \text{ and } \forall q_{\lambda_D} \in H^{-1/2}(\Gamma_D)^d, \\ a(q,p) + \langle \mathcal{D}_u \mathcal{I}(u,p,n), q \rangle + \displaystyle\int_\Omega \langle \mathcal{D}_u \mathcal{M}(u,x), q \rangle \, \mathrm{d}x + \int_{\partial\Omega} \langle \mathcal{D}_u \mathcal{N}(u,x), q \rangle \, \mathrm{d}s(x) \\ = \displaystyle\int_{\Gamma_D} (p_{\lambda_D} \cdot q + (p - p_{\alpha_D} n_y) \cdot q_{\lambda_D} - p_{\lambda_D} \cdot n_y q_{\alpha_D}) \, \mathrm{d}s(x). \end{cases} \tag{79}$$

4.4 Finite element discretization and fictitious domains method

To compute each direct and adjoint problem on the evolving domain Ω^k, we use a fictitious domain method with respect to the fixed domain $\mathcal{D}$ containing Ω^k. The fictitious domains method used in this work is close to the Xfem approach [40]. It is presented in [31, 9] and applied to the unilateral contact and to Nitsche's method in [23]. One of the main advantages of this method is its optimal convergence, including when a high-order base finite element method is used. It mainly consists in considering a classical finite element method, here a Lagrange P_2 finite element on the polar grid also used for the level set discretization, and taking its restriction on the real domain Ω^k. Consequently, only one fixed, regular and polar grid is manipulated for the level set and the finite element method. As an illustration, Figure 7 successively depicts an example of a polar structured mesh of the fictitious domain $\mathcal{D}$, the mesh cut by the level set representing Ω^k and the computed direct solution u_{Ω^k} using a Lagrange P_2 cut finite element method.

The discretized non-linear direct problems are solved with a non-smooth Newton-Raphson algorithm. The finite element software used for the analysis is GetFEM++ [48] with its python interface.

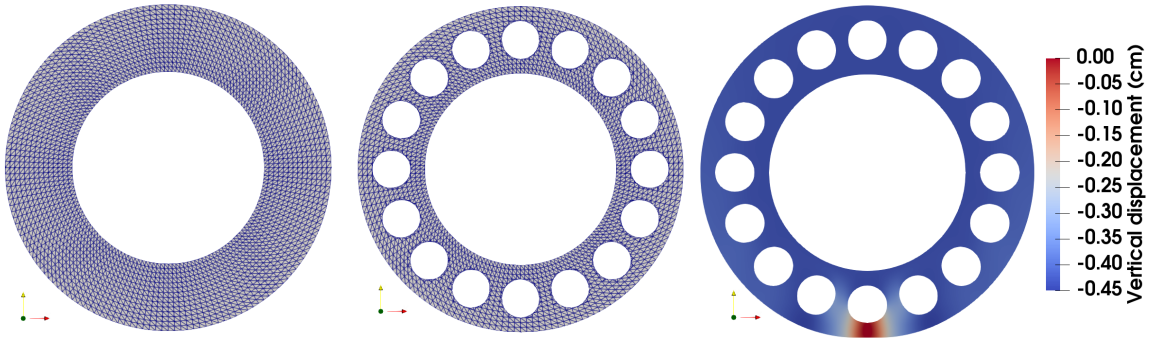

Figure 7: Left to right: the structured polar mesh, the mesh cut by the level set representing Ω^k and a direct solution u_{Ω^k} plot on the deformed mesh.

It has been noted in [31, 9] that an optimal approximation of the gradient of the solution is not achieved in the cut element method without the addition of a stabilization term, mainly on elements having a very small intersection with the real domain Ω^k, as illustrated in Figure 8. Since the computation of the shape gradient requires the computation of the gradient of the displacement on the level set itself, we added a stabilization term to ensure a good quality of the approximation. We have chosen to use the so-called ghost penalty method proposed by E. Burman and P. Hansbo in [8] which aims at penalizing some inter-element jumps, on the elements cut by the level set. A stabilization term is added to the direct problem which then reads

$$\begin{cases} \text{Find } u \in H^1(\Omega) \text{ such that} \\ a(u,v) + \mathcal{I}(u,v,n) + G(u,v,n) = \ell(v), \end{cases} \tag{80}$$

where G is the ghost penalty term

$$G(u,v,n) = \sum_{E\in\mathcal{E}^k} \frac{1}{2}\int_E \frac{\xi}{\gamma}[\![\sigma(u)n]\!]\cdot[\![\sigma(v)n]\!]\,\mathrm{d}s(x), \tag{81}$$

where $\mathcal{E}^k$ denotes the set of edges (for $d=2$) or faces (for $d=3$) of the mesh having a non empty intersection with $\partial\Omega^k$, $[\![\sigma(u)\cdot n]\!]$ denotes the inter-element stress jump over E, n is a unit normal vector to E and ξ is the penalty parameter. The same term is imposed on the adjoint equation (43) and reads

$$\langle \mathcal{D}_u\, G(u,p,n), q\rangle = \sum_{E\in\mathcal{E}^k} \frac{1}{2}\int_{\partial T} \frac{\xi}{\gamma}[\![\sigma(q)n]\!]\cdot[\![\sigma(p)n]\!]\,\mathrm{d}s(x). \tag{82}$$

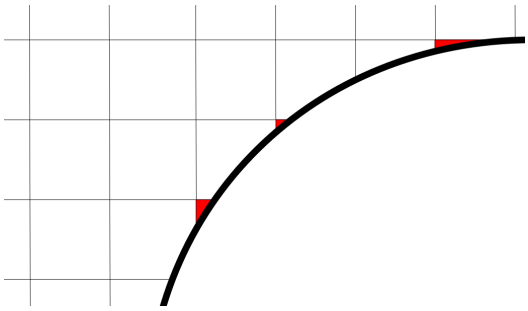

Figure 8: Example of a structured mesh at the interface with a hole. The red areas depict cut elements having a small intersection with the domain Ω^k where the gradient of the solution may be of poor quality.

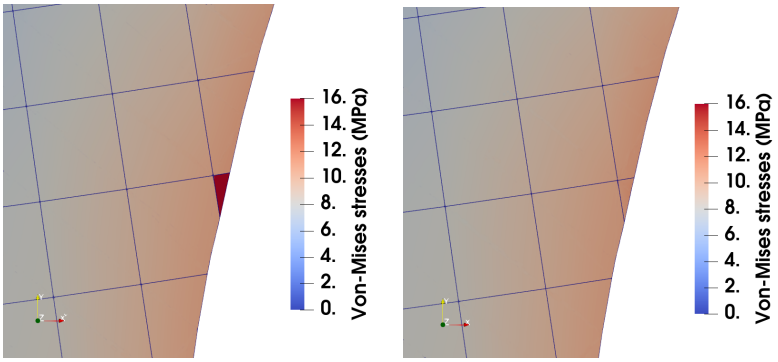

Figure 9: Focus on the Von Mises stress of two solutions of the direct problem near a hole. On the left the stress jump is not penalized to compute the solution ($\xi = 0$) and on the right the stress jump is penalized ($\xi = 10^{-3}$).

To illustrate the influence of the stabilization parameter, Figure 9 shows that the stress (here the Von-Mises stress) can be badly estimated on the elements having a very small intersection with the real domain in the absence of a stabilization term ($\xi = 0$), whereas the application of a small stabilization term ($\xi = 10^{-3}$) allows to recover a good approximation. In the following, all the computations are performed with a penalization parameter $\xi = 10^{-3}$.

5 Numerical experiments

In this section, we present a set of numerical tests, beginning with a simple initial geometry. The objective is successively to evaluate the difference in behavior of the penalty and Nitsche methods for the approximation of the contact condition, and to evaluate the different criteria of uniformization of the contact force density. Finally, we illustrate the shape optimization on more complex initial geometries.

5.1 Geometry setting

We consider the domain presented in Figure 6 which is a ring with an inner radius $R_i = 20$ cm and an outer radius $R_e = 34$ cm containing sixteen regularly spaced holes of radius $r = 4$ cm. The ring width is set to $w_r = 12$ cm. The domain is divided in $N_s = 16$ sectors for periodic simplification. We compute $N_d = 8$ mechanical load positions per sector. The Young modulus is set to $E = 200$ MPa and the Poisson ratio is $\nu = 0.48$. A contact might occur on the boundary Γ_C upon the outer radius R_e with a flat rigid body representing the ground. A load condition is set on the rigid boundary Γ_D upon the inner radius R_i and the load is supposed to be 300 kg. We only present frictionless tests as friction does not influence the optimal shapes we obtained in our tests, in the absence of horizontal load.

5.2 Minimization of the sole elastic strain energy

A first optimization is performed on the simple initial geometry with only a minimization of the elastic strain energy J_e. The result is presented in Figure 10 for a contact condition approximated by Nitsche's method with parameters $\gamma = E/h_T$ and $\theta = -1$.

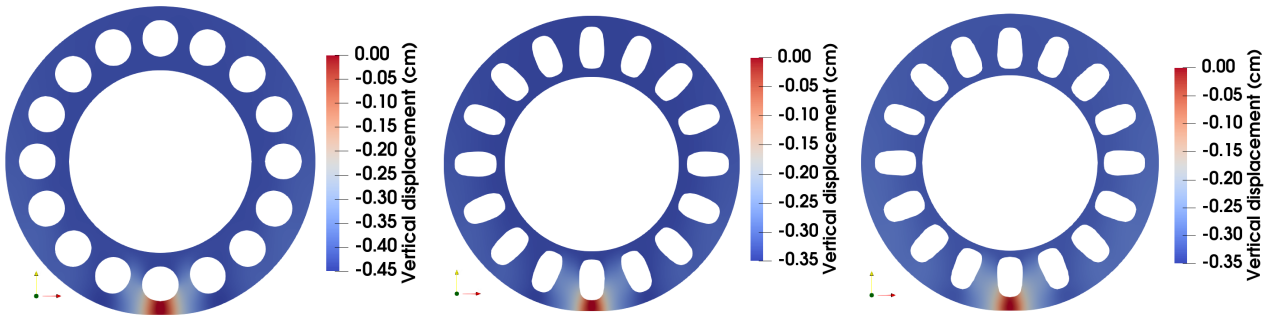

Figure 10: Shape optimization for the sole strain energy. The vertical displacement is displayed. Contact treated by Nitsche's method. From left to right: first iteration, 20th iteration and 100th iteration.

The circular holes progressively radially lengthen along the optimization process to bring stiffness and to reduce deformation whatever the load position is. The evolution of the objective function J_e is presented in Figure 11.

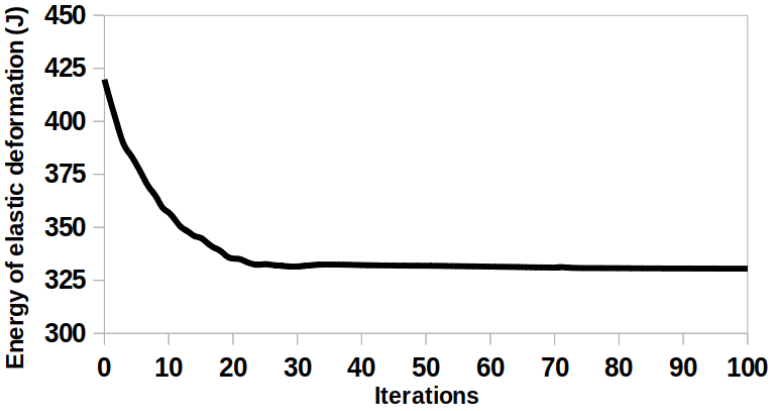

Figure 11: Evolution of the elastic strain energy J_e for the configuration presented in Figure 10 according to the successive iterations of the shape optimization algorithm.

5.3 Comparison of contact methods for the geometric shape optimization

In order to compare the two strategies to account for the contact condition, the test of the previous section is now performed using the penalty method to treat the contact. The penalty parameter is also taken equal to $\gamma = E/h_T$. The result of the shape optimization is shown in Figure 12.

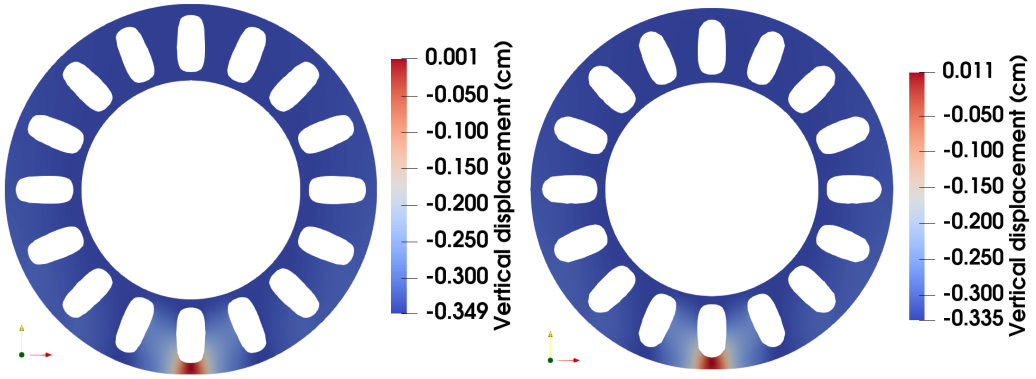

Figure 12: Optimal shapes for different contact methods. On the left: optimal shape with the contact treated by penalization and on the right: optimal shape with the contact treated by Nitsche's method.

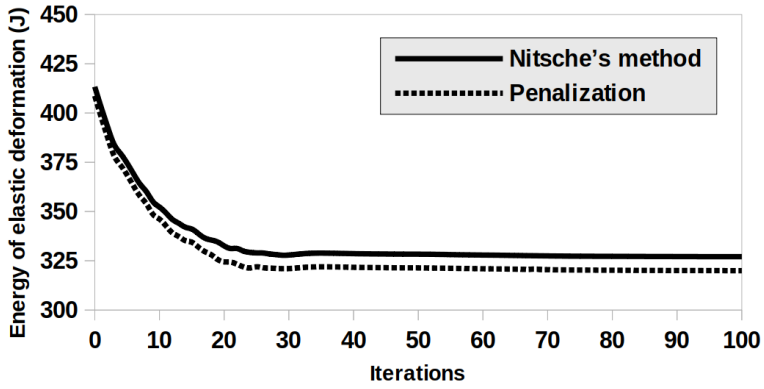

Figure 13: Evolution of the strain energy J_e during the shape optimization: comparison between Nitsche's method and penalization.

It can be noted, comparing with Figure 10 that both methods almost lead to the same final and optimal shape. A very careful comparison shows that the solution with penalty corresponds to a slightly higher deflection of the structure. The difference is more significant in Figure 13 where a comparison of the evolution of elastic strain energy is plotted for the two methods. With the penalty, the elastic strain energy is underestimated because of the interpenetration. To overcome this drawback, the penalty parameter γ might be increased so that the contact would be better estimated. Two other tests are performed with $\gamma = 10E/h_T$ for both methods. The optimal shape and deformation obtained can be seen in Figure 14. The two deformations are very close to each other in that case and the evolution of the strain energy, plotted in Figure 15 is also almost the same. The main conclusion that can be drawn by considering the result presented in Figure 15 is that the use of the penalty method leads to a shape optimization more sensitive to the parameter γ than Nitsche's method whose results are quite independent of γ. The consideration of Nitsche's method thus allows the use of a parameter γ with a smaller value without deteriorating the quality of the solution. It also allows to avoid some potential difficulties which can be encountered when γ is large and which can result in a stiff problem difficult to solve numerically. As a consequence of this comparison, for the rest of our numerical study, we use Nitsche's method with a parameter $\gamma = E/h_T$.

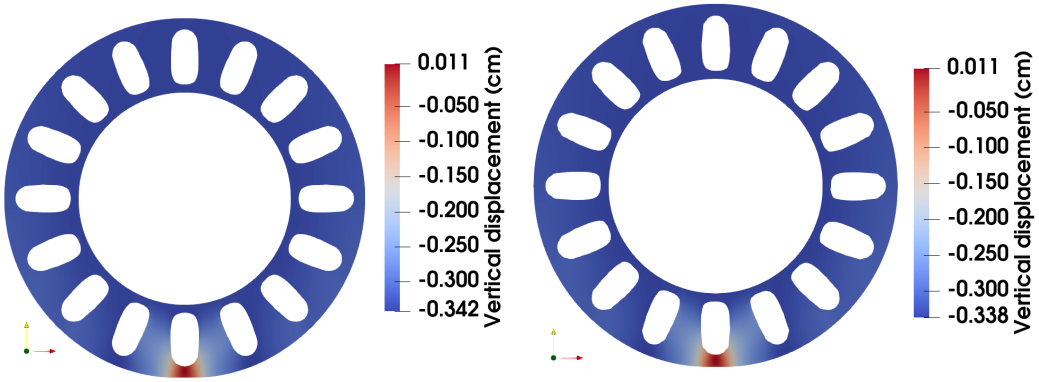

Figure 14: Optimal shapes for different contact methods. $\gamma = 10E/h_T$. On the left: optimal shape with the contact treated by penalization and on the right: optimal shape with the contact treated by Nitsche's method.

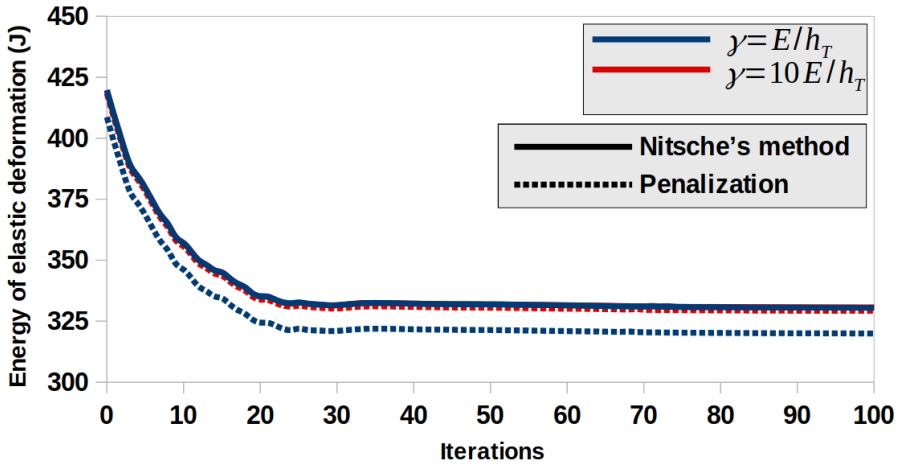

Figure 15: Evolution of the strain energy J_e during the shape optimization: comparison between Nitsche's method and penalization and different values of the parameter γ.

5.4 Comparison of contact criterion strategies

A comparison is led between the contact stress criterion strategies described earlier. We recall that to uniformize the contact stress between the successive load positions, two strategies were presented in the previous parts: either the contact boundary is thickened with a size ϵ which leads to the criterion $J_{p,1}$ given by (60), or we consider the norm $H^{-1/2}(\Gamma_C, \mathbb{R}^d)$ of the criterion $J_{p,2}$ given by (61). We also recall that the general criterion set in the optimization algorithm reads as in (5). Here, the characteristic length L is chosen to be equal to ϵ. To perform a comparison between the two strategies $J_{p,1}$ and $J_{p,2}$, the parameter α is chosen to reach the same criterion amplitude at the first iteration of the optimization on both contact criterion strategies, i.e.

$$\sum_{i=1}^{N_d} \alpha_1 J_{p,1}(\Omega^0, u^i_{\Omega^0}, p_{mean}) = \sum_{i=1}^{N_d} \alpha_2 J_{p,2}(\Omega^0, u^i_{\Omega^0}, p_{mean}). \tag{83}$$

To this aim, we take in our case a weight $\alpha_1 = 6$ for the criterion $J_{p,1}(\Omega, u^i, p_{mean})$ and a weight $\alpha_2 = 100$ for $J_{p,2}(\Omega, u^i, p_{mean})$. In order to measure the effect of the uniformization criteria, Figure 16 first gives the optimal shape and the contact stress curves on the different positions without using these criteria (i.e. with $\alpha = 0$). One can see a significant disparity of contact stresses on the different loading positions which obviously corresponds to the presence or not of a hole near the effective contact area.

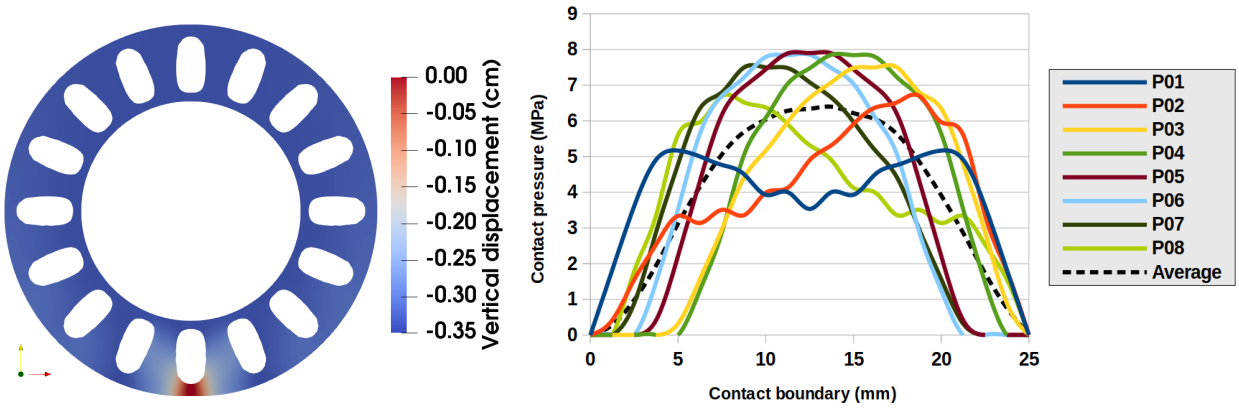

Figure 16: Optimization with J_e ($\alpha = 0$). Contact treated by Nitsche's method. On the left: optimal shape and on the right: contact stresses on the 8 load positions.

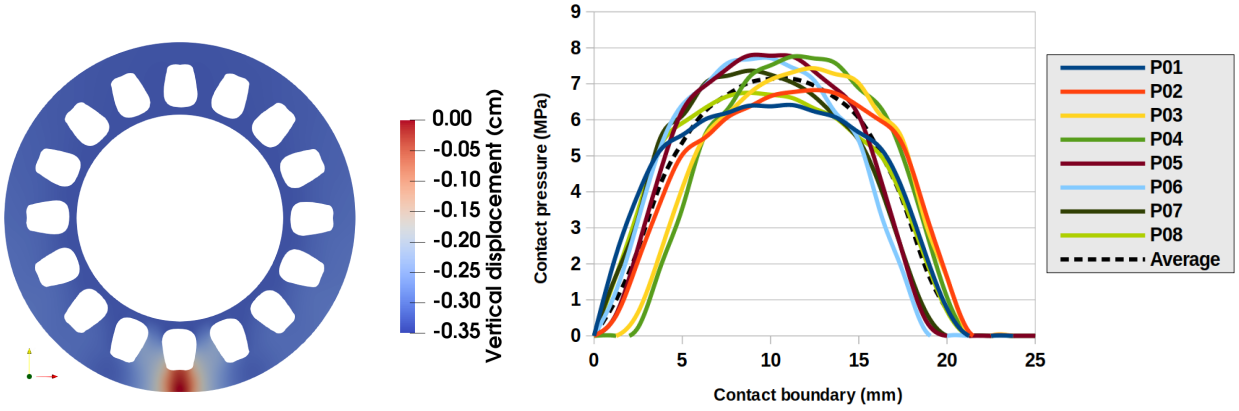

Figure 17: Optimization with J_e and $J_{p,1}$ ($\alpha_1 = 6$). Contact treated by Nitsche's method. On the left: optimal shape and on the right: contact stress on the 8 load positions.

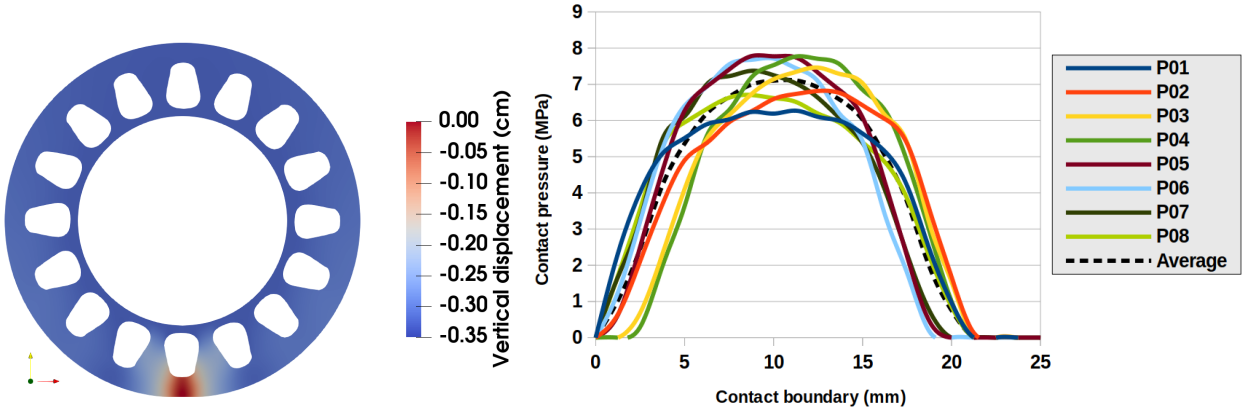

Figure 18: Optimization with J_e and $J_{p,2}$ ($\alpha_2 = 100$). Contact treated by Nitsche's method. On the left: optimal shape and on the right: contact stresses on the 8 load positions.

The effect of the addition of the uniformization criteria can be seen in Figures 17 and 18 for $J_{p,1}$ and $J_{p,2}$, respectively. Both criteria give some similar results, in particular the disparities on contact

stresses have been significantly reduced compared to Figure 16 when only the strain energy is used. One of the effect of both criteria is a certain radial transfer of the holes away from the contact boundary resulting in some thickening of the ring of material located between the contact boundary Γ_C and the holes. It is quite obvious that this transfer contributes to the desired uniformization. One also notes a slight difference between the shapes obtained with $J_{p,1}$ and $J_{p,2}$, the thickening being a little bit more important for $J_{p,1}$ and ending with a smaller amount of material between the holes. There is also a difference in the decrease of the two criteria that is presented in Figure 19, $J_{p,2}$ having a proportionally larger decrease which shows that $J_{p,2}$ is actually a bit more efficient than $J_{p,1}$. In particular, one advantage of the criterion $J_{p,2}$ over $J_{p,1}$ is that it does not depend on the parameter ϵ. And so, the calculation with $J_{p,2}$ does not require a non-optimizable zone of thickness ϵ which is more natural than the calculation with $J_{p,1}$ in this mechanical study.

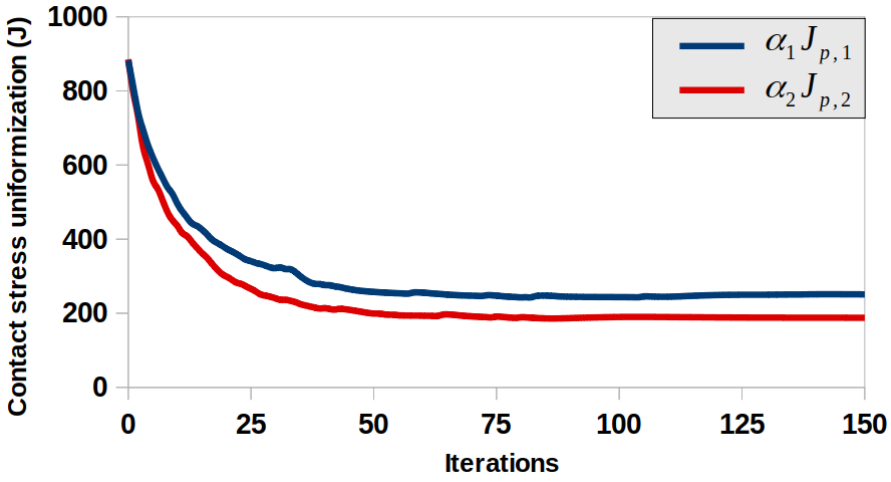

Figure 19: Comparison between the contact criterion strategies $J_{p,1}$ and $J_{p,2}$. Evolution of the contact stress uniformization criteria $J_{p,1}$ and $J_{p,2}$ for the configurations presented in Figures 17 and 18.

The parameter α_2 influences the optimization and the minimization of J_e and $J_{p,2}$. One notes that $\alpha_2 = 10$ leads to a light optimization of $J_{p,2}$ as shown in Figure 20 whereas $\alpha_2 = 1000$ leads to a good uniformization of the contact stress even though the deflection of the structure increases (see Figure 21), and so J_e is less minimized. A wise choice of $\alpha_2 = 100$ is a good compromise to minimize both J_e and $J_{p,2}$ for this configuration (see Figure 18).

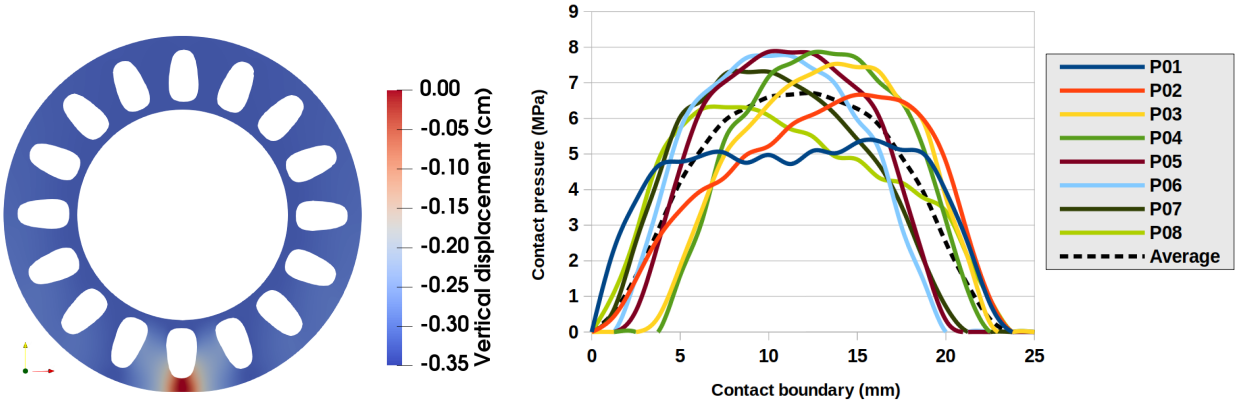

Figure 20: Optimization with J_e and $J_{p,2}$ ($\alpha_2 = 10$). Contact treated by Nitsche's method. On the left: optimal shape and on the right: contact stresses on the 8 load positions.

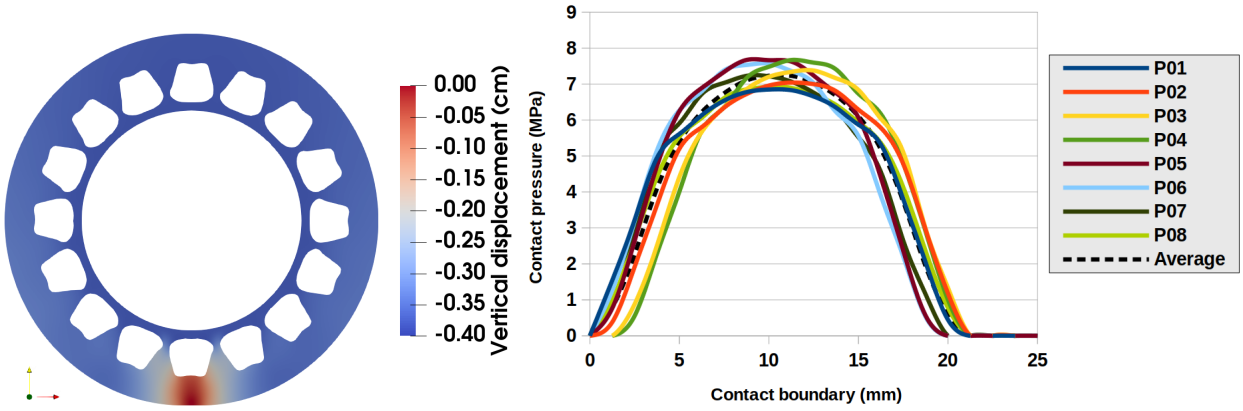

Figure 21: Optimization with J_e and $J_{p,2}$ ($\alpha_2 = 1000$). Contact treated by Nitsche's method. On the left: optimal shape and on the right: contact stresses on the 8 load positions.

5.5 Shape optimization of complex geometries

It is obvious that the final geometry obtained by shape optimization depends on the chosen initial geometry. This is especially the case since we have chosen to constrain the amount of material to remain constant. To illustrate the variety of shapes that can be obtained, optimization results are presented on Figure 22 with or without the use of an uniformization criterion of the contact stress and for an initial geometry with 48 holes. Finally, we present a case with an initial geometry with 108 holes optimized for the sole strain energy in two-dimensional and three-dimensional configurations in Figure 23.

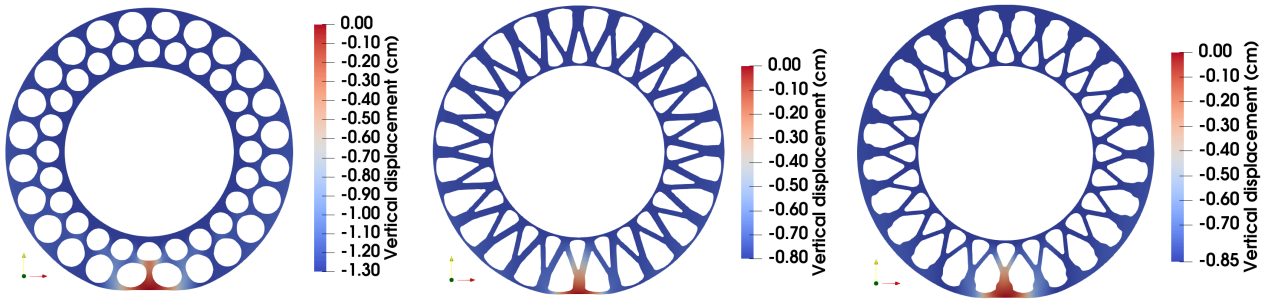

Figure 22: Optimal designs for 48 initial holes. From left to right: initial geometry with 48 circular holes, optimization with the J_e energy criterion and a multi-criterion optimization with J_e and $J_{p,2}$ with $\alpha = 50$.

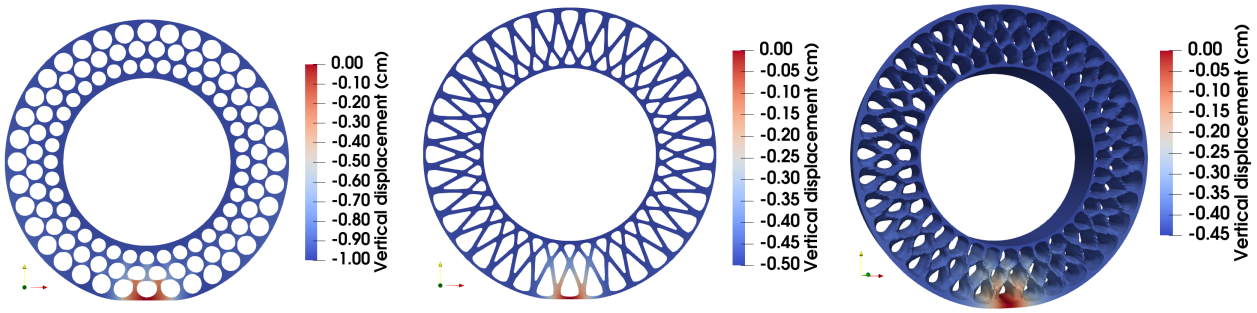

Figure 23: Optimal designs for 108 initial holes with the minimization of the J_e energy criterion. From left to right: initial two-dimensional geometry with 108 circular holes, a two-dimensional optimal shape and a three-dimensional optimal shape.

6 Conclusion

In this paper, we have presented a strategy for the shape optimization of a linearly elastic rolling structure in contact with a flat ground.
The main ingredients was Nitsche's method for the contact approximation, the use of cut finite elements, a level set representation of the geometry approximated on a regular polar grid and Sethian's schemes for its evolution. More precisely, the cut finite element method was used on the regular grid for the approximation of the displacement fields and the adjoint variables. Indeed, thanks to its optimal convergence, it allows the use of a coarser grid than for other fictitious domain methods. Finally, the ghost penalty stabilisation allows us to obtain a good quality gradient on the boundary of the evolving domain.
Beyond these choices, we have presented comparisons of the treatment of the contact condition by penalty and by Nistche's method. In particular, these numerical experiments highlight the advantage of Nitsche's method which allows a consistent approximation of the contact condition without the use of Lagrange multipliers. We have also introduced two variants of a criterion for the uniformization of the contact stress for which, the associated adjoint state is well defined and has a continuous dependence on the data. Finally, the numerical experiments using each of these two criteria show very similar optimal elastic structures.
The natural perspectives of this work are the transition to large elastic deformations and the mathematical study of differentiability of objective functions which we plan to address in a future work.

Acknowledgements

We are grateful for the acknowledgement of the French National Association for Research and Technology (ANRT, CIFRE grant number 2019/1027). This work was also supported by the MFP MICHELIN.

References

[1] R. A. Adams and J. JF Fournier. *Sobolev spaces*. Elsevier, 2003.

[2] P. Alart and A. Curnier. A mixed formulation for frictional contact problems prone to Newton like solution methods. *Computer methods in applied mechanics and engineering*, 92(3):353–375, 1991.

[3] G. Allaire, F. Jouve, and A.-M. Toader. A level-set method for shape optimization. *Comptes Rendus Mathematique*, 334:1125–1130, 06 2002.

[4] G. Allaire, F. Jouve, and A.-M. Toader. Structural optimization using sensitivity analysis and a level-set method. *Journal of Computational Physics*, 194(1):363 – 393, 2004.

[5] A. Amassad, D. Chenais, and C. Fabre. Optimal control of an elastic contact problem involving Tresca friction law. *Nonlinear Analysis*, 48(8):1107–1135, 2002.

[6] V. Barbu. Optimal control of variational inequalities. *Research Notes in Math.*, 100, 1984.

[7] P. Beremlijski, J. Haslinger, J. V. Outrata, and R. Pathó. Shape optimization in contact problems with Coulomb friction and a solution-dependent friction coefficient. *SIAM Journal on Control and Optimization*, 52(5):3371–3400, 2014.

[8] E. Burman and P. Hansbo. Edge stabilization for the generalized stokes problem: a continuous interior penalty method. *Computer methods in applied mechanics and engineering*, 195(19-22):2393–2410, 2006.

[9] E. Burman and P. Hansbo. Fictitious domain finite element methods using cut elements: I. a stabilized Lagrange multiplier method. *Computer Methods in Applied Mechanics and Engineering*, 199(41-44):2680–2686, 2010.

[10] E. Burman and P. Hansbo. Fictitious domain finite element methods using cut elements: Ii. a stabilized Nitsche method. *Applied Numerical Mathematics*, 62(4):328–341, 2012.

[11] J. Cea. Conception optimale ou identification de formes, calcul rapide de la dérivée directionnelle de la fonction coût. *ESAIM: Mathematical Modelling and Numerical Analysis - Modélisation Mathématique et Analyse Numérique*, 20(3):371–402, 1986.

[12] B. Chaudet-Dumas and J. Deteix. Shape derivatives for the penalty formulation of elastic contact problems with Tresca friction. *SIAM Journal on Control and Optimization*, 58(6):3237–3261, 2020.

[13] B. Chaudet-Dumas and J. Deteix. Shape derivatives for an augmented Lagrangian formulation of elastic contact problems. *ESAIM: Control, Optimisation and Calculus of Variations*, 27:S14, 2021.

[14] F. Chouly. An adaptation of Nitsche 's method to the Tresca friction problem. *Journal of Mathematical Analysis and Applications*, 411(1):329–339, 2014.

[15] F. Chouly, M. Fabre, P. Hild, R. Mlika, J. Pousin, and Y. Renard. An overview of recent results on Nitsche's method for contact problems. In *Geometrically unfitted finite element methods and applications*, pages 93–141. Springer, 2017.

[16] F. Chouly and P. Hild. A Nitsche-Based method for unilateral contact problems: Numerical analysis. *SIAM J. Numerical Analysis*, 51:1295–1307, 2013.

[17] F. Chouly, P. Hild, V. Lleras, and Y. Renard. Nitsche-based finite element method for contact with Coulomb friction. In *European Conference on Numerical Mathematics and Advanced Applications*, pages 839–847. Springer, 2017.

[18] F. Chouly, P. Hild, and Y. Renard. Symmetric and non-symmetric variants of Nitsche's method for contact problems in elasticity: theory and numerical experiments. *Mathematics of Computation*, 84(293):1089–1112, 2013.

[19] U. Clarenz, U. Diewald, and M. Rumpf. *Anisotropic geometric diffusion in surface processing.* IEEE, 2000.

[20] M. Cocu. Existence of solutions of Signorini problems with friction. *International journal of engineering science*, 22(5):567–575, 1984.

[21] G. Duvaut and J. L. Lions. *Les inéquations en mécanique et en physique*. Dunod, 1972.

[22] C. Eck and J. Jarusek. Existence results for the static contact problem with Coulomb friction. *Mathematical Models and Methods in Applied Sciences*, 8(03):445–468, 1998.

[23] M. Fabre, J. Pousin, and Y. Renard. A fictitious domain method for frictionless contact problems in elasticity using Nitsche's method. *The SMAI journal of computational mathematics*, 2:19–50, 2016.

[24] J. Hadamard. *Mémoire sur le problème d'analyse relatif à l'équilibre des plaques élastiques encastrées*, volume 33. Imprimerie nationale, 1908.

[25] J. Haslinger. Signorini problem with Coulomb's law of friction. shape optimization in contact problems. *International Journal for Numerical methods in engineering*, 34(1):223–231, 1992.

[26] J. Haslinger and A. Klarbring. Shape optimization in unilateral contact problems using generalized reciprocal energy as objective functional. *Nonlinear Analysis: Theory, Methods & Applications*, 21(11):815–834, 1993.

[27] J. Haslinger and R. AE Mäkinen. *Introduction to shape optimization: theory, approximation, and computation*. SIAM, 2003.

[28] J. Haslinger and P. Neittaanmäki. On the existence of optimal shapes in contact problems. *Numerical Functional Analysis and Optimization*, 7(2-3):107–124, 1985.

[29] J. Haslinger, P. Neittaanmäki, and T. Tiihonen. Shape optimization in contact problems based on penalization of the state inequality. *Aplikace matematiky*, 31(1):54–77, 1986.

[30] J. Haslinger, J. V. Outrata, and R. Pathó. Shape optimization in 2D contact problems with given friction and a solution-dependent coefficient of friction. *Set-Valued and Variational Analysis*, 20(1):31–59, 2012.

[31] J. Haslinger and Y. Renard. A new fictitious domain approach inspired by the extended finite element method. *SIAM Journal on Numerical Analysis*, 47(2):1474–1499, 2009.

[32] A. Henrot and M. Pierre. *Variation et optimisation de formes: une analyse géométrique*, volume 48. Springer Science & Business Media, 2006.

[33] P. Hild. Non-unique slipping in the Coulomb friction model in two-dimensional linear elasticity. *Quarterly Journal of Mechanics and Applied Mathematics*, 57(2):225–235, 2004.

[34] P. Hild. Multiple solutions of stick and separation type in the Signorini model with Coulomb friction. *ZAMM-Journal of Applied Mathematics and Mechanics/Zeitschrift für Angewandte Mathematik und Mechanik: Applied Mathematics and Mechanics*, 85(9):673–680, 2005.

[35] J. Jarušek. Contact problems with bounded friction. coercive case. *Czechoslovak Mathematical Journal*, 33(2):237–261, 1983.

[36] N. Kikuchi and J. T. Oden. *Contact problems in elasticity: a study of variational inequalities and finite element methods*. SIAM, 1988.

[37] J. L. Lions. *Contrôle optimal de systèmes gouvernés par des équations aux dérivées partielles*. Dunod, 1968.

[38] A. Maury, G. Allaire, and F. Jouve. Shape optimisation with the level set method for contact problems in linearised elasticity. *hal-01435325v2*, 2017.

[39] F. Mignot. Contrôle dans les inéquations variationelles elliptiques. *Journal of Functional Analysis*, 22(2):130–185, 1976.

[40] N. Moës, J. Dolbow, and T. Belytschko. A finite element method for crack growth without remeshing. *International journal for numerical methods in engineering*, 46(1):131–150, 1999.

[41] F. Murat and J. Simon. Etude de problèmes d'optimal design. In *IFIP Technical Conference on Optimization Techniques*, pages 54–62. Springer, 1975.

[42] J. Nitsche. Über ein variationsprinzip zur lösung von Dirichlet-problemen bei verwendung von teilräumen, die keinen randbedingungen unterworfen sind. *Abhandlungen aus dem Mathematischen Seminar der Universität Hamburg*, 36:9–15, 1971.

[43] S. J. Osher and J. A. Sethian. Fronts propagating with curvature-dependent speed: Algorithms based on Hamilton-Jacobi formulations. *Journal of Computational Physics*, 79(1):12 – 49, 1988.

[44] S.J. Osher and F. Santosa. Level set methods for optimization problems involving geometry and constraintsi. frequencies of a two-densityinhomogeneous drum. *Journal of Computational Physics*, 171:272–288, 2001.

[45] O. Pironneau. Optimal shape design for elliptic systems. In *System Modeling and Optimization*, pages 42–66. Springer, 1982.

[46] K. Poulios and Y. Renard. An unconstrained integral approximation of large sliding frictional contact between deformable solids. *Comput. Struct.*, 153(C):75–90, June 2015.

[47] Y. Renard. A uniqueness criterion for the Signorini problem with Coulomb friction. *SIAM journal on mathematical analysis*, 38(2):452–467, 2006.

[48] Y. Renard and K. Poulios. GetFEM: Automated FE modeling of multiphysics problems based on a generic weak form language. *Transactions on Mathematical Software*, 47:1, 2020.

[49] J. A. Sethian. *Level set methods and fast marching methods: evolving interfaces in computational geometry, fluid mechanics, computer vision, and materials science*, volume 3. Cambridge university press, 1999.

[50] J. Simon. Differentiation with respect to the domain in boundary value problems. *Numerical Functional Analysis and Optimization*, 2(7-8):649–687, 1980.

[51] J. Sokolowski and J.-P. Zolésio. Shape sensitivity analysis of unilateral problems. *SIAM journal on mathematical analysis*, 18(5):1416–1437, 1987.

[52] J. Sokolowski and J.-P. Zolésio. Introduction to shape optimization. In *Introduction to Shape Optimization*, pages 5–12. Springer, 1992.

[53] M. Sussman, P. Smereka, and S. J. Osher. A level set approach for computing solutions to incompressible two-phase flow. *Journal of Computational Physics*, 114(1):146–159, 1994.